THE EFFECT OF SUPPORT TYPE ON WATER-GAS SHIFT KINETICS OVER Pt BASED TRIMETALLIC SYSTEMS

by
Nijat İbrahimov
B.Eng. Chemical Engineering, The University of Birmingham, 2017

Submitted to the Institute for Graduate Studies in
Science and Engineering in partial fulfillment of
the requirements for the degree of
Master of Science

Graduate Program in Chemical Engineering
Boğaziçi University
2020

to my family

ACKNOWLEDGEMENTS

Firstly, I would like to thank my thesis supervisor Prof. Ahmet Erhan Aksoylu, who never hesitated to support and give his valuable advice anytime throughout my master's study at Boğaziçi University. His guidance, motivation and encouragement during all these years are highly appreciated. Working with him was a privilege for me, since I learned many things from his experience and professionalism in catalysis and reaction engineering.

I would like to express my sincere appreciations for the members of thesis committee, Prof. Ramazan Yıldırım and Assoc. Prof. Alper Uzun for devoting their valuable time to read and comment on my thesis.

Special thanks to Dr. Burcu Selen Çağlayan for her excellent guidance, willingness to help and giving priceless suggestions on this work.

I would like to thank my dearest and lovely friends, Semih Altınsoy, Gülten Çelebi and Uğurcan Tozar for sharing all the good and bad moments with me and for giving me continuous encouragement and friendship. Deepest thanks to Ali Uzun, Merve Eropak and Burcu Acar for their everlasting help and guidance throughout this study. I also wish to express my gratitude to all members of CATREL team, that I pride to work with.

Most importantly, I wish to thank my family for all their support, patience and encouragement not only during my studies at university but also throughout my life. Their never-ending love and trust in me made me motivated all the time.

Finally, the financial support provided by Presidency of the Republic of Turkey, Department of Strategy and Budget (Ministry of Development) through projects 2016K12-2838 (2016K121160), and by TÜBİTAK through project 214M170 are gratefully acknowledged.

ABSTRACT

The Effect of Support Type on Water-Gas Shift Kinetics over Pt-Based Trimetallic Systems

The aim of the current study is to determine the power law type rate expressions of water-gas shift (WGS) reaction over 1Pt-1Re-1Na/CeO_2 and 1Pt-1Re-1Na/TiO_2 catalysts under realistic feed conditions. In this context, the 1Pt-1Re-1Na/CeO_2 and 1Pt-1Re-1Na/TiO_2 samples were prepared by using sequential incipient-to-wetness impregnation (IWI) method. The preliminary kinetic tests were conducted to determine the experimental conditions guaranteeing kinetically controlled and mass transfer limitation free zone. The kinetic experiments were performed at 350 °C and an atmospheric pressure, with H_2O/CO feed ratio ranging between 15 and 45. For each sample, 15 pairs of kinetic experiments, for which partial pressures of CO, H_2O, H_2, CO_2 and CH_4, and residence time (W_{cat}/F_{CO}) were changed according to an experimental design. The values for the experimental initial rates were used to evaluate kinetic parameters of the power law type rate expressions. The reaction orders for CO, H_2O, H_2 and CO_2 were calculated as 0.79, 0.24, -0.30 and -0.31, respectively, within ±7% error over the CeO_2 supported catalyst through non-linear regression analysis in MATLAB^{TM}, while the orders were estimated as 0.57, 0.45, -0.30 and -0.32 for the same sequence over the TiO_2 supported sample within ±9% error. This study also revealed that changes in CH_4 partial pressure have negligible effect on the reaction rates obtained for both samples. Based on the reaction orders estimated for both catalysts, it can be concluded that CeO_2 supported sample is more sensitive to CO, which is more likely due to high oxygen storage capacity of ceria, while the opposite is true for TiO_2. The apparent activation energies and the frequency factors were calculated as 51.07 kJ mol^{-1} and 947.90 μmol mg_{cat}^{-1} s^{-1} $kPa^{-0.42}$, respectively for 1Pt-1Re-1Na/CeO_2, while those were found to be 69.53 kJ mol^{-1} and 446.01 μmol mg_{cat}^{-1} s^{-1} $kPa^{-0.40}$ for 1Pt-1Re-1Na/TiO_2, in the temperature range of 300-350 ºC.

ÖZET

Destek Tipinin Pt-Bazlı Üç Metalli Sistemler Üzerindeki Su-Gaz Değişim Kinetiğine Etkisi

Bu çalışmanın amacı, gerçekçi besleme koşulları altında pratik üssel hız denklemlerini kullanarak 1Pt-1Re-1Na/CeO_2 ve 1Pt-1Re-1Na/TiO_2 katalizörleri üzerinde su-gaz değişim reaksiyonunun kinetiğini belirlemektir. Bu kapsamda, 1Pt-1Re-1Na/CeO_2 ve 1Pt-1Re-1Na/TiO_2 katalizörleri sıralı IWI impregnasyon yöntemi kullanılarak hazırlandı. Kinetik olarak kontrol edilen ve kütle transferi sınırlamaları olmayan bölgeyi garanti edecek deney koşullarını belirlemek için ön kinetik testleri yapıldı. Kinetik deneyler, 350°C'lik bir çalışma sıcaklığında ve 15 ile 45 arasında değişen H_2O/CO besleme oranlı atmosferik basıncında yürütülmüştür. Her katalizör için, 15 çift kinetik deney CO, H_2O, H_2, CO_2 ve CH_4 kısmi basınçları ve reaktörde kalma süresi, (W_{cat}/F_{CO}) değiştirilerek gerçekleştirilmiştir. Deneysel başlangıç hız değerleri, üssel hız denklemlerinin kinetik parametrelerini belirlemek için kullanılmıştır. CeO_2 destekli katalizör için, sırasıyla CO, H_2O, H_2 ve CO_2 üssel değerleri %7 hata içerisinde MATLAB^{TM} de doğrusal olmayan regresyon analizi uygulanarak 0.79, 0.24, -0.30 ve -0.31 olarak hesaplanmıştır. Bununla birlikte, TiO_2 destekli numune için 0.57, 0.45, -0.30 ve -0.32 değerleri aynı reaksiyon bileşenlerinin sırası için %9 hata içerisinde tahmin edilmiştir. Bu çalışma aynı zamanda CH_4 kısmi basıncındaki değişikliklerin her iki numune için elde edilen reaksiyon hızları üzerinde ihmal edilebilir bir etkisi olduğunu ortaya koydu. Her iki katalizör için tahmin edilen üssel değerleri dikkate alındığında, CeO_2 desteğinin yüksek oksijen depolama kapasitesi nedeniyle CO'ya karşı daha duyarlı olduğu halde, bunun tersi de TiO_2 desteği için doğru olduğu sonucuna varılabilir. Görünür aktivasyon enerjileri ve frekans faktörleri 300-350 ºC sıcaklık aralığında, 1Pt-1Re-1Na/CeO_2 için sırasıyla 51.07 kJ mol^{-1} ve 947.9 μmol $mgcat^{-1}$ s^{-1} $kPa^{-0.42}$ olarak hesaplanırken, 1Pt-1Re-1Na/TiO_2 için sırasıyla 69.53 kJ mol^{-1} ve 446.01 μmol $mgcat^{-1}$ s^{-1} $kPa^{-0.40}$, olarak bulunmuştur.

TABLE OF CONTENTS

LIST OF FIGURES

LIST OF TABLES

LIST OF SYMBOLS

E_A	Activation Energy
F	Flow rate
k	Rate constant
k_0	Pre-exponential factor
K_{eq}	Equilibrium constant
m_{cat}	Catalyst weight
$n_{i,in}$	Molar flow rate of component i in the feed stream
$n_{i,out}$	Molar flow rate of component i in the product stream
P	Pressure
r	Reaction rate
R	Universal gas constant
T	Temperature
vol	Volume
W_{cat}	Catalyst weight
wt	Weight
X	Conversion
α	Reaction order of carbon monoxide
β	Reaction order of steam
β’	Factor of reversible reaction
δ	Reaction order of hydrogen
γ	Reaction order of carbon dioxide
ε	Reaction order of methane
ΔH°_{298}	Standard enthalpy of reaction

LIST OF ACRONYMS/ABBREVIATIONS

ATR	Autothermal Reforming
CATREL	Catalysis and Reaction Engineering Laboratory
DI	Deionized
DRIFT	Diffuse Reflectance Infrared Fourier Transform Spectroscopy
FC	Fuel Cell
FP	Fuel Processor
FTIR	Fourier Transform Infrared Spectroscopy
GC	Gas Chromatograph
GDC	Gadolinium Doped Ceria
GHSV	Gas Hourly Space Velocity
HPLC	High Performance Liquid Chromatography
HTS	High Temperature Shift
ID	Inner Diameter
LTS	Low Temperature Shift
MFC	Mass Flow Controller
MS	Mass Spectrometry
OD	Outer Diameter
OSC	Oxygen Storage Capacity
OSR	Oxidative Steam Reforming
PEM	Proton Exchange Membrane
PEMFC	Proton Exchange Membrane Fuel Cell
PGM	Platinum Group Metal
PID	Proportional Integral Derivative
POX	Partial Oxidation
PROX	Preferential Oxidation
RWGS	Reverse Water Gas Shift
SR	Steam Reforming
SS	Stainless Steel
TCD	Thermal Conductivity Detector

TOF	Turn-over Frequency
TOS	Time-on-stream
TOX	Total Oxidation
WGS	Water-Gas Shift

1. INTRODUCTION

Producing sufficient amount of energy for the world's growing demands and its associated environmental challenges are twin issues, requiring serious attention nowadays. A big dilemma existing today is that there is a growing interest in finding new sustainable energy sources and routes, yet the continuous exploitation of fossil fuels is necessary to meet the growing demands together with its environmental costs. Currently, a large amount, about two thirds of the world's energy requirement is met by conventional liquid and gaseous fuels, such as petroleum and natural gas due to their prevalent availability and well-established distribution systems. The utilization of non-renewable fossil-based natural resources, especially in the power and transport industries, causes worries due to rise in emissions of pollutants, resulting in a deteriorating impact on our eco-systems. Recent research on the future energy sources to replace fossil fuels has revealed many other alternative options such as biodiesel, methanol, synthetic natural gas (SNG), hydrogen and so forth. Alternative energy sources and production routes are to be investigated in order to effectively solve both the energy security and climate change issues (Sigh *et al*., 2015; Ahmed *et al*., 2016).

Meeting the 21st century's energy demands and keeping levels of pollution as low as possible to minimize the medium-term risk of climate change could rather be fulfilled by an energy carrier with no or very little environmental impact. In this sense, hydrogen could be considered as a promising energy carrier to address the aforementioned problems as it owns the following advantageous features: (i) hydrogen when combusted with oxygen releases energy and pure water as the sole reaction product; (ii) not only fossil fuels, but also renewables are the natural sources, which hydrogen can be derived from; (iii) hydrogen may be used in different applications such as centralized or decentralized energy production systems (Cipriani *et al*. 2014). Since hydrogen has technological hurdles in its storage and distribution, on-site hydrogen production from hydrocarbons using the fuel processors (FP) combined with fuel cell (FC) technologies seems as an alternative option to the above-mentioned problems. In the near future, the combined fuel processor – proton exchange membrane fuel cell (FP–PEMFC) systems used in electricity production for small-scale stationary applications are anticipated to become an essential part of the

distributed energy production systems. PEMFCs, which are used for small-scale stationary applications such as combined heat and power generation, can be considered as one of the most practical fuel cell types with a higher efficiency and a lower operating temperature range compared to other fuel cell types (Eropak and Aksoylu, 2017).

In a typical fuel processor, generally three processes, the steam reforming (SR)/auto-thermal reforming (ATR)/oxy-steam reforming (OSR), water-gas shift (WGS) and preferential oxidation (PROX) are conducted in series. The feed containing a hydrocarbon fuel, oxygen and water mixture is fed to the first reactor of the FP, the OSR reactor, where endothermic steam reforming and exothermic oxidation reactions take place simultaneously generating a gas which is rich in H_2 yet containing side products such as CO and CO_2.

The gas mixture rich in H_2, also called syngas, produced via the OSR reaction contains CO, which is a potential poison for Pt-based electro-catalysts of the PEMFC. Therefore, the CO concentration in syngas needs to be lowered down to 100 ppm or below prior to entering the PEMFC in order to protect electrodes from CO poisoning. The syngas clean-up process is performed by WGS reaction, reducing the CO concentration down to 0.5–1vol.%, followed by a final CO removal step – PROX reaction, dropping CO content down to ppm levels (Ercolino *et al*., 2015).

First discussed in 1888, the WGS reaction became well-known with the Haber ammonia synthesis process, but now is generally used to produce methanol, hydrogen and hydrocarbons (through the Fischer-Tropsch process). The WGS reaction is a reversible and moderately exothermic reaction, where CO reacts with H_2O to generate CO_2 and H_2. Increasing temperature shifts the equilibrium constant of the WGS reaction towards reactants (H_2O and CO) and increases the reaction rate. However, it is thermodynamically more favorable at low temperatures (Saeidi *et al*., 2017).

In industrial applications, WGS is conventionally conducted in two consecutive stages namely, the high temperature shift (HTS) and low temperature shift (LTS) reactors as the reaction is kinetically more favorable at high temperatures, while thermodynamically more promising at low temperatures. At elevated temperatures, the

carbon monoxide (CO) conversion is restricted due to the equilibrium; however, the reaction rate can be increased by carrying out the reaction at a high temperature. The temperature of the gas stream leaving the high temperature WGS reactor is raised to about 400 ^{o}C, and the CO concentration in the gas mixture is reduced down to 2-3 vol.%. Catalysts used for the HTS reaction are iron-based catalysts typically promoted with chromium oxide for stability due to the possible loss in their activity at elevated temperatures (Opalka *et al*., 2008). The gas stream leaving the second stage reactor, LTS unit, is at about 200 ^{o}C and the CO concentration in the gas mixture is reduced to less than 0.6 vol.%. Conventional catalysts used for the LTS reaction are mainly Cu supported on alumina and promoted with ZnO to have longer lifetime (Gradisher *et al*., 2015).

While the copper–zinc LTS catalysts are widely used in large-scale chemical industries, specific care and safety cautions must be taken into account during the reduction process of those catalysts as they are pyrophoric, if exposed to air. The above-mentioned drawbacks of the copper-based traditional catalysts can effectively be controlled in the hydrogen production plants, whereas those catalysts are not suitable for small-scale stationary applications such as FP-PEMFC systems. The requirements for the WGS catalysts used in FP-PEMFC systems differ from their conventional alternatives. The WGS catalysts to be used in FPs should have (i) sufficient resistant to air exposure and operate effectively at HTS-LTS transition temperature range (i.e. 250-400 ^{o}C), (ii) high activity leading significant reduction in the reactor volume and weight, and (iii) an adequate tolerance to frequent start-up/shut-down cycles and maintain their original performance. Noble metal (Pt or Au) based catalysts have been investigated to meet the aforementioned requirements for a successful catalyst (Castano *et al*., 2014).

Kinetic expressions for WGS reaction on different feed compositions and catalysts are important to determine the reaction rates under various operating conditions and hence, design the reactor with an optimal size. In the current work, which is a successor of the former WGS performance studies conducted by our group (Eropak, B.M., 2020) on the sequentially impregnated Pt-Re-Na metals on two different supports (CeO_2 and TiO_2), the practical power law type rate expressions have been determined for CeO_2 and TiO_2 supported Pt-Re-Na systems, and the developed expressions were comparatively analyzed to elucidate the effect of support type on the kinetics of WGS reaction.

In this study, Chapter 2 gives a detailed literature survey about the fuel processors and fuel cell technologies, the WGS reaction and conventional and noble metal-based catalysts developed for the target reaction, followed by the kinetics of WGS reaction. In the experimental part (Chapter 3), all materials (chemicals, liquids and gases) used in this study, the experimental systems used for catalyst preparation, catalytic reaction and product analysis, and kinetic tests are covered. The results of current study are presented and discussed in Chapter 4. Finally, the conclusions of the present study and recommendations for further studies are briefly described in Chapter 5.

2. LITERATURE SURVEY

2.1. The Fuel Cell and Fuel Processor Technologies

A fuel cell is an electrochemical device converting the chemical energy of various fuels (e.g. hydrogen, methane and alcohols) into electric power without combustion and is considered as one of the most favorable power production systems, as it operates in a reliable and environmentally friendly way with high efficiency in energy conversion and requires very little maintenance during its lifetime. Depending upon the electrolyte type, fuel cells can be classified as polymer electrolyte membrane fuel cells (PEMFCs), solid oxide fuel cells (SOFCs), alkaline membrane fuel cells (AMFCs), etc. (Wang *et al*., 2018).

Among other types of fuel cells, the hydrogen-fueled proton exchange membrane fuel cells (PEMFCs) are considered as the most favorable option to produce electricity more efficiently for small-scale applications. Because of the technological hurdles in hydrogen storage, the on-site hydrogen production through the fuel processor (FP) systems using various hydrocarbon fuels with well-established distribution grids is thought as an immediate solution to deliver hydrogen fuel for PEMFCs (Gökaliler *et al*., 2008).

Hydrogen, which is considered as an ideal fuel for PEMFCs, is fed into the fuel cell system and gets ionized into protons and electrons on the surface of the anode. Passing through the membrane, the produced protons reach the opposite electrode to make the water formation reaction take place on the surface of cathode. In PEMFCs, the electrodes primarily made of platinum material are unable to resist against contaminants such as carbon monoxide (CO). The CO poison of the electrodes is more likely to occur if the carbon monoxide contamination level is above 40 ppm. Therefore, the design of fuel processors must be adequate in such a way that it can satisfy the requirements set for the CO contamination level (Trimm and Önsan, 2011).

Since PEMFCs require pure hydrogen to effectively operate, the purification of the hydrogen-rich gas stream from its impurities must be a selective process involving a sequence of catalytic reactions taking place in fuel processor systems. In this sense, in a

typical fuel processor, the successive reactions to produce highly pure hydrogen almost free from CO contaminants may include the reforming reaction of hydrocarbons, the water-gas shift (WGS) reaction to decrease carbon monoxide content and enrich hydrogen concentration and the preferential carbon monoxide oxidation (PROX) reaction to reduce carbon monoxide content further to a ppm level at which the electrodes of PEMFCs are not deteriorated by CO (Çağlayan and Aksoylu, 2009).

2.1.1. The Reforming Reaction of Hydrocarbons

Steam reforming (SR), partial oxidation (POX), and autothermal reforming (ATR) are the three principal methods applied in converting hydrocarbons into the hydrogen-rich product stream. Through the reforming reaction, a gas mixture, consisting mainly of H_2, CO and CO_2, is produced. For the endothermic steam reforming of hydrocarbons, heat is supplied to the system externally, and compared to POX and ATR, this reaction requires a lower operating temperature. As defined in Equation 2.1, the SR generates a product stream with a high H_2/CO ratio, making it desirable for hydrogen production, but not suitable for the onboard FP-FC systems due to a requirement for a large reactor (Holladay *et al*., 2009).

$$C_nH_m + nH_2O \rightarrow nCO + \left(n + \frac{m}{2}\right)H_2 \quad (2.1)$$

In the partial oxidation reaction, a hydrocarbon fuel reacts with a stoichiometric amount of pure oxygen as defined in Equation 2.2 below. For several reasons, for example, a requirement for a smaller reactor size, having adequate response time and being less sensitive to fuel variation, partial oxidation can be preferred to the steam reforming reaction. Another comparison between partial oxidation and steam reforming can be made for the reaction rate, in which case, partial oxidation of methane takes place faster than the steam-methane reforming (SMR) reaction. The conversion of hydrocarbons to synthesis gas (CO + H_2) via the partial oxidation reaction can be conducted at elevated temperatures in the absence of catalysts, but the operating temperature will considerably be lowered, if the reaction is catalyzed (Sengodan et al., 2018).

$$C_nH_m + \frac{1}{2}nO_2 \rightarrow nCO + \frac{m}{2}H_2 \quad (2.2)$$

The auto-thermal reforming (ATR) or oxidative steam reforming (OSR) reaction, which is a combination of the endothermic SR and exothermic POX reactions, is practical in handling the coke formation and attaining a thermally neutral medium. The carbon formation on the conventional and precious metal-based catalysts is one of the key problems encountered in the SR reaction, leading to the activity loss in the catalysts. Besides this, steam reforming of the heavier hydrocarbons has much more tendency to coke formation compared to methane. However, unlike the SR reaction, the presence of oxygen in the ATR/OSR process can reduce the coke formation by gasifying the carbon deposits (Cui and Kaer, 2018).

2.1.2. The Water-Gas Shift Reaction

A gaseous mixture, mostly comprising of hydrogen (H_2), carbon monoxide (CO) and carbon dioxide (CO_2), is produced through the reforming reactions. The amount of CO present in the reformate gas stream from the reforming unit is lowered down by the WGS reaction, which also yields an additional amount of hydrogen in the product stream. Through this reaction, a mixture of CO and water steam is converted to CO_2 and H_2 as described in Equation 2.3:

$$CO + H_2O \leftrightarrow CO_2 + H_2 \qquad \Delta H^{\circ}_{298} = -41.2\ \text{kJ/mol} \quad (2.3)$$

An increase in the operating temperature of the slightly exothermic WGS reaction subsequently results in a decline in its equilibrium constant. From the thermodynamic point of view, carrying out the reaction at lower temperatures shift the equilibrium towards the products, but the reaction is kinetically desirable to be performed at higher temperatures.

According to the Le Chatelier's principle, any changes in the pressure of the system does not have any effect on the equilibrium. The WGS reaction is crucial in the clean-up process of hydrogen, which helps to reduce carbon monoxide levels down to 0.5-1 vol.%.

As the presence of CO in the feed stream to the PEMFCs can deactivate the platinum electrodes, the WGS reaction is applied to reduce CO concentrations and maximize the hydrogen output for the fuel cell applications (Pal *et al*., 2018).

2.1.3. The Preferential Oxidation Reaction

Following the water-gas shift reaction, small amount of CO ($\sim 0.5 - 1$vol.%) is still present in the product stream leaving the WGS reactor. This hydrogen-rich gas stream, intended to be used as a fuel in PEMFCs, still contaminated with carbon monoxide and can subsequently pollute the platinum anodes of the fuel cells as a result of an irreversible adsorption of CO molecules on the Pt surfaces. Hence, the CO concentration must be reduced to an acceptable level at which the performance of PEM fuel cells is not affected. To lower the CO levels down to 100 ppm or less, the preferential oxidation of CO (PROX) has been reported as an economical, reliable and safe method for the in-situ hydrogen production in fuel processors. The reactions taking place in a PROX reactor are defined in Equations 2.4 and 2.5 below (Venkata *et al*., 2018):

$$CO + {}^{1}/_{2}\, O_2 \rightarrow CO_2 \qquad \Delta H^{\circ}_{298} = -283\ \text{kJ/mol} \tag{2.4}$$

$$H_2 + {}^{1}/_{2}\, O_2 \rightarrow H_2O \qquad \Delta H^{\circ}_{298} = -242\ \text{kJ/mol} \tag{2.5}$$

The conversion of carbon monoxide to carbon dioxide reaction (Equation 2.4) is the desirable one, which is typically carried out at lower temperatures. However, the oxidation reaction of hydrogen (Equation 2.5) is unwanted and a competitive reaction taking place at higher temperatures. Hence, H_2 oxidation must be minimized while the CO concentration is reduced to a tolerable level (less than 100 ppm). Generally, the PROX reaction is performed with slightly surplus air supply consistent with the CO/O_2 molar ratio. From the thermodynamic point of view, the enthalpy of the hydrogen oxidation reaction is less than that of the CO oxidation reaction, but as the temperature increases, H_2 hinders CO adsorption on the active sites of the catalyst. (Mohamed *et al*., 2016).

2.2. WGS Catalysts

The water-gas shift, being a slightly exothermic, reversible and equilibrium-limited reaction, has an important role in reducing the CO content in the product stream leaving the reforming unit down to 0.5 – 1 vol.% to protect the PEMFC electrodes from poisoning and simultaneously increasing the hydrogen concentration in the reformate stream (Pasel *et al*., 2018).

In order to achieve high performance in terms of CO conversion, the WGS reaction is conventionally carried out at two different operating temperatures. In industrial applications, the iron-based catalysts are used for the first stage, the high temperature water-gas shift (HT-WGS) reaction, typically operating in the temperature range of 350–450 °C, while the copper-based catalysts are practical for the low temperature water-gas shift (LT-WGS) reaction operating within 190–250 °C. The reason is that Fe-based catalysts lose their catalytic activity at low temperatures while the Cu-based catalysts prone to sintering at elevated temperatures. In recent years, noble metal-based catalysts with a medium operating temperature are being developed to overcome the aforementioned problems (Zhu and Wachs, 2018).

Due to the stringent limitations set for the reactor size and cost and concerns about the pyrophoricity and lengthy pre-conditioning process, the commercial high and low temperature WGS catalysts are not considered appropriate for the small-scale immobile fuel processor – fuel cell (FP-FC) systems. In the normal operation of an FP-FC system, it experiences frequent start-up/shut-down rotations which are the processes leading to sharp temperature changes, water condensation and vaporization. Therefore, during the start-up/shut-down processes, the catalysts get deactivated faster compared to the steady-state operation (Guo *et al*., 2009). On the other hand, WGS catalysts used for hydrogen clean-up for the fuel cell applications are required to be active at low temperatures (i.e. below 300 °C). Among the catalysts investigated so far, the noble metal-based catalysts have been reported as good candidates for the small-scale stationary FP-FC systems (Xu *et al*., 2015).

2.2.1. Conventional WGS Catalysts

The method applied in the synthesis of catalysts has a considerable effect on their performance. Under the low temperature WGS reaction conditions, Jeong *et al*. (2014) studied the catalytic performance of the ceria supported Cu-based catalysts prepared by the incipient wetness impregnation and co-precipitation methods. They synthesized two 20 wt% copper loaded on ceria catalysts via the incipient-to-wetness impregnation and one-step co-precipitation techniques. According to the WGS performance test results, the latter demonstrated better activity and stability compared to the impregnated Cu/CeO_2 catalyst. It was also reported that the co-precipitated Cu/CeO_2 has perfect CO_2 selectivity and that the high activity and stability of this catalyst are closely related to its ease of reducibility and high surface availability. The effect of titration time on the catalytic performance of Cu/CeO_2, prepared by a simple precipitation technique, was investigated by Na *et al*. (2018) for the WGS reaction. They determined that the physical properties such as specific surface area and crystallite size of the support are affected by the time spent on the titration process. The results of WGS reaction over the Cu/CeO_2 catalysts, synthesized by applying different titration times, revealed that the Cu/CeO_2–0 (where 0 indicates the instant addition of precipitant into the $Ce(NO_3)_3$ solution) has the highest activity. This is primarily due to the availability of oxygen vacancies, high specific surface area, good active metal dispersion over the support and the ease of catalyst reducibility.

In another study of WGS activity over copper-based catalysts by Zhang *et al*. (2014), the zirconia supported Cu-based catalysts with three different copper loadings were prepared using the deposition-precipitation technique and tested under the so-called reaction conditions. On the synthesized CuO/ZrO_2 catalysts, three kinds of CuO species were determined: (i) highly dispersed CuO molecules which are weakly linked to ZrO_2; (ii) strongly bound Cu-[O]-Zr through the ZrO_2 surface oxygen vacancy; and (ii) crystalline CuO. The amount of Cu-[O]-Zr species is related to the reaction rate and possibly, responsible for the attainment of high activity in the CuO/ZrO_2 catalysts. According to the results of inductively coupled plasma optical emission spectrometry and TPR by hydrogen, it was revealed that amount of Cu-[O]-Zr species in CuO/ZrO_2 catalysts corresponds to the Cu loading order of 6.1 wt.% > 8.4wt.% > 4.1wt.%.

Another catalyst synthesis method was investigated by Yan *et al*. (2018), who prepared Cu-Fe_3O_4 and Cu-Fe_3O_4-Al_2O_3 catalysts via an aerosol-spray self-assembly method and tested their performance under the WGS reaction conditions. They reported that both the Cu-Fe_3O_4 and Cu-Fe_3O_4-Al_2O_3 catalysts prepared by the so-called method show very good WGS activity. This is explained by the addition of Fe, which significantly improves the Cu^0 dispersion and leads to a better reducibility as a result of the interaction between the copper and iron atoms. Hence, the Fe addition resulted in the promotion of WGS activity. They concluded that the Cu-Fe_3O_4-Al_2O_3 catalyst is a superior candidate for the WGS reaction compared to Cu-Fe_3O_4 one.

2.2.2. Noble Metal-based WGS Catalysts

The commercial WGS catalysts (Fe– and Cu-based catalysts) do not show sufficient stability in the oxidizing environment or high activity at relatively low temperatures, therefore, they are not applicable for the small-scale stationary fuel cell applications (Jeong *et al*., 2013). However, recent studies on WGS catalysts revealed that the noble metals (Pt, Au, Ru, Rh and Pd) supported on reducible oxides like TiO_2, CeO_2, ZrO_2 are more practical in the fuel cell applications as they are able to overcome the limitations of the conventional WGS catalysts (Rodriguez, 2011).

The role of active metal, Au, in the Au-Co_3O_4/CeO_2 catalyst was evaluated by Gamboa-Rosales *et al*. (2016) for the WGS and oxygen enriched WGS reactions. They reported that the addition of gold particles facilitates the CeO_2 and Co_3O_4 reducibility and has a positive effect on the oxygen storage capacity of the catalyst, owing to the interaction between the Au and Co species. It was also found that the addition of oxygen in WGS reaction promotes the performance of both Au-based and Au free catalysts within 190-350 ^oC and helps to produce more hydrogen, making the oxygen enriched WGS reaction more desirable for hydrogen production processes.

Soria *et al*. (2014) studied a series of Fe_2O_3 supported gold catalysts, prepared by three different methods, namely, double impregnation, deposition-precipitation and liquid phase reductive deposition methods and tested for the low temperature WGS reaction. The Au/Fe_2O_3 catalysts synthesized via the deposition-precipitation process exhibited higher

CO conversion compared to other two methods investigated. It was reported that gold particles facilitate the reducibility of the Fe_2O_3 support and very good active metal dispersion over the iron support is obtained for the deposition-precipitation method, based on the results of the temperature programmed reduction by hydrogen and high-resolution transmission electron microscopy.

The catalytic performance of Au/TiO_2 catalysts, prepared by double impregnation, deposition-precipitation and liquid phase reductive deposition techniques were evaluated under the low temperature WGS conditions (Perez *et al*., 2016). Various amounts of Au particles with a maximum loading of 2.5 wt.% were added onto the support. A comparison between the catalysts synthesized by different techniques was performed based on the CO conversion and turnover frequency. The best catalytic performance was obtained for Au/TiO_2 catalysts with a gold loading of 2.5wt.% synthesized by deposition precipitation and liquid phase reductive deposition methods. Since the Au/TiO_2 catalyst prepared by liquid phase reductive deposition process is easily affected by deactivation, the Au/TiO_2 produced through deposition precipitation can be considered as a better choice (with CO conversion of 85%) under the examined operating conditions (at 300 ^oC and 1 atm).

Vindigni *et al* (2012) prepared various gold-based catalysts with different Au loadings supported on ceria only and the mixture of ceria and zirconia and studied their WGS performance at low temperatures. They found that Au particles supported on the oxide mixtures (CeO_2-ZrO_2) have better catalytic activity compared to Au/CeO_2, following the activity sequence of $Au/CeO_2(50)$-$ZrO_2(50)$ >$Au/CeO_2(80)$-$ZrO_2(20)$ >Au/CeO_2. The study evidenced that Au dispersion and the amount of zirconia added are closely related with each other. The best catalytic activity was obtained for $Au/CeO_2(50)$-$ZrO_2(50)$, which is associated with the presence of many gold nanoparticles and the effect of ZrO_2 addition. The FTIR analysis revealed that before and after the reaction the carbon residuals have the lowest stability over the $Au/CeO_2(50)$-$ZrO_2(50)$ catalyst, making it the most stable one among the catalysts investigated.

A study comparing the WGS reaction performance for the Au–Re/CeO_2, Au/CeO_2 and Re/CeO_2 catalysts was carried out by Çağlayan and Aksoylu (2011). They reported that Au loaded by deposition precipitation method on the impregnated Re/CeO_2 catalyst

results in well-dispersed gold species strongly interacting with rhenium. However, in case of the Re impregnation on the deposition precipitated Au/CeO_2 catalyst, the activity becomes lower than that observed in the former case. This can be justified in a way that the blockage of the active sites occurs in the case of Re impregnation over Au/CeO_2. Amongst the catalysts investigated, the one synthesized by 1wt.% Au deposition precipitated and 0.5wt.% Re impregnated on ceria support was recommended as the optimal catalyst for the target reaction performed with high steam to carbon ratios.

In another study, the WGS activity of the bimetallic Au–Me/CeO_2 catalysts (where Ni, Cu, Ag, Pt, and Pd are indicated as Me), each synthesized by the sequential impregnation technique, was examined by Yu *et al*. (2010). Compared to other bimetallic systems investigated in their study, the Au–Pt/CeO_2 sample demonstrated higher catalytic activity with a carbon monoxide conversion of 78% at an operating temperature of 250 ^oC. This is explained by the presence of platinum and gold species in the Au–Pt/CeO_2 bimetallic catalyst and their interaction with each other and the support, resulting in the formation of oxygen vacancies and partially oxidized Au particles.

A comparison between the gold- and platinum-based catalysts was made by Castano *et al*. (2014). In their work, the WGS reaction performance of the Au- and Pt-based catalysts supported on CeO_2-Al_2O_3 and $Ce_{0.8}Fe_{0.2}$-Al_2O_3 was investigated. They reported that independent of the feed composition, the Au-based samples show higher catalytic activity than the Pt-based alternatives at an operating temperature of 180 ^oC. However, according to the results of their study, the Pt-based catalysts can be considered more practical than the Au-based samples, as they can tolerate to changes in the feed composition with high turnover frequencies and achieves the equilibrium at an operating temperature of 250 ^oC.

Jeong *et al*. (2013) performed a study to compare CeO_2, ZrO_2 and CeO_2-ZrO_2 supported Pt catalysts namely, Pt/CeO_2, Pt/ZrO_2, and Pt/$Ce_{(1-x)}Zr_{(x)}O_2$), under the WGS reaction conditions in the temperature range of 200 – 360 ^oC. As per the results of their work, the platinum supported on ceria only (Pt/CeO_2) demonstrated a higher turnover frequency and a lower activation energy value for the WGS reaction. It was also observed that this sample stays stable for longer time than the other Pt-based catalysts investigated in

this study. Hence, Pt/CeO_2 catalyst was recommended as a favorable option for the low temperature WGS reaction due to its aforementioned advantages.

Pt-Mo/SiO_2 catalysts synthesized by Xu *et al*. (2015) via the impregnation-reduction technique demonstrated higher CO conversion for the WGS reaction compared to Pt/SiO_2 samples at an operating temperature ranging between 150 ^oC and 300 ^oC. In this study, it was determined that the addition of Mo particles encourages the platinum dispersion over the support and enhances the interaction between the Pt and MoO_x particles, which in turn leads to an increased WGS activity. The platinum species promoted by well-dispersed MoO_x oxides were considered as active building blocks for the reaction.

In a study by Rodriguez *et al*. (2017), the WGS performance of Pt/MoC and Pt/TiC samples was tested at temperatures of 410, 425, 435, 450 and 465 K. Their study revealed that Pt/MoC and Pt/TiC catalysts are highly active, stable for long time and selective towards the reaction products, which makes them superior over the commercial Cu-based WGS catalysts. This is clarified by the interaction between the metals and carbides, leading to a better catalytic activity. The increased activity is explained by the fact that the Pt/MoC and Pt/TiC samples can partly dissociate H_2O molecules.

The type of treatment procedures applied during the pre-conditioning or activation processes has a significant effect on the performance of catalysts. In this sense, Perez *et al*. (2018) prepared the Pt/CeO_2 catalyst by the incipient-to-wetness impregnation method and treated the catalyst by cold argon plasma to study its performance under the WGS reaction conditions. The activation process was carried out by air calcination, reduction by hydrogen and cold argon plasma treatment. They reported that the catalyst treated by the combination of air calcination, Ar plasma and H_2 reduction gives high CO conversions. The analysis of the catalyst structure and its performance revealed that the plasma treatment resulted in electron-enriched Pt particles which strongly interact with the CeO_2 support. This, consequently, promotes the ceria reducibility and hence, the CO conversion.

The effect of support type (CeO_2, TiO_2 and CeO_2-TiO_2) on the WGS activity of Pt-based catalysts was studied by Gonzalez *et al*. (2010). According to their experimental results, platinum metal supported on CeO_2-TiO_2 demonstrated higher activity and longer

stability than the pure CeO_2 and TiO_2 supported catalysts. The characterization analysis of Pt/CeO_2-TiO_2 revealed that cerium in the CeO_2-TiO_2 support is well-dispersed and closely interacts with titanium particles. Furthermore, the interaction between the Pt and Ce species makes the reducibility of CeO_2 easier in the Pt/CeO_2-TiO_2 catalyst at low temperatures. Hence, the ease of reducibility of Pt/CeO_2-TiO_2 is considered as the reason for this catalyst to be highly active and stable under the WGS reaction conditions.

The secondary metal or promoter added to the noble metal-based catalysts has a noticeable effect on the catalytic activity. In this context, Zhu *et al*. (2011) synthesized Pt-Na/TiO_2 catalysts with 1wt.% Pt and different Na loadings by the co-impregnation method and evaluated their catalytic performance for the WGS reaction. The researchers reported that a considerable increase in the catalytic activity is obtained for the sodium addition ranging between 2 and 4 wt.%. The contact between the primary metal, Pt and the secondary metal, Na forms highly active sites at the interface of $Pt–NaO_x$ and prevents platinum species from sintering. It was concluded that 4 wt.% Na is the most favorable amount for sodium addition, which enhances the WGS activity and turnover frequency.

Another research group, Sato *et al*. (2005) investigated the effect of a promoter addition, rhenium on platinum, palladium and iridium supported on TiO_2 under the WGS reaction conditions. They observed an increase in the activity of the catalysts upon addition of Re particles, which can be explained by the possible electron exchange between the active metals and the promoter in the Pt-Re/TiO_2, Pd-Re/TiO_2 and Ir-Re/TiO_2 samples. The analysis of adsorbed catalysts by fourier-transform infrared spectroscopy showed that alike configurations of the active sites can possibly be formed between the primary metals and rhenium, which activates the water molecules and speeds up the water-gas shift reaction.

2.3. WGS Kinetics

The study of WGS reaction kinetics for different feed compositions and catalysts are practical in the determination of the reaction rates under different operating conditions and hence, making right decisions on reactor design tradeoffs.

2.3.1. Kinetics of Conventional WGS Catalysts

A study on the kinetics of conventional WGS catalysts was carried out by Plaza *et al*. (2016), who developed two power law type rate expressions for the CoO/MoO_3 and Fe_2O_3/CrO_3 oxides supported on γ-Al_2O_3 to study the effect of partial pressures of the reaction components and temperature on the WGS kinetics. Over the Co/Mo-based catalyst, the reaction orders were obtained as 1.28, 0.03, -0.11 and -0.35 for CO, H_2O, CO_2 and H_2, respectively at an operating temperature of 380 ^oC, whereas 1.37, 0.23, -0.16 and -0.11 were evaluated for the same sequence of components over the Fe/Cr-based catalyst at 300 ^oC. The activation energy value for the Co/Mo-based sample was calculated as 66 kJ/mol in the temperature range of 320 – 470 ^oC and that for the Fe/Cr-based catalyst was found to be 102 kJ/mol within 220 – 305 ^oC. The effect of H_2S addition (at 100 vol.ppm) on the power-law type rate expression was also examined. The study recommended that at the given amount of H_2S, the Fe/Cr-based catalyst is preferable over the Co/Mo-based one, since the presence of sulfur does not affect the activity of the Fe/Cr-based catalyst as long as the temperature is kept above 315 ^oC.

The empirical power law type expressions over two commercial iron–chromium based catalysts, namely, HTC1 (80-90wt% Fe_2O_3, 8-13wt% Cr_2O_3, 1-2wt% CuO) and HTC2 (80-95wt% Fe_2O_3, 5-10wt% Cr_2O_3, 1-5% CuO) were defined by Hla *et al*. (2009) under the WGS reaction conditions. They carried out the kinetic tests at a temperature and a pressure of 450 ^oC and 1 atm, respectively. As per the results of their study, HTC1 was found to be more practical for the feed streams with high CO concentrations, since the reaction order of CO (1.0) over this sample is greater than that of HCT2 (0.9). However, in case of a WGS feed stream containing large amount of CO_2, HCT2 can be considered more practical as it has less negative power value for CO_2 (-0.156) compared to HCT1 (-0.36).

The synthesis of new catalysts that can operate at a temperature well above that of conventional high temperature WGS catalysts and the development of rate expressions for those catalysts have become a challenging subject in recent years. In this context, Hla *et al*. (2011) prepared a new perovskite-like catalyst ($La_{0.7}Ce_{0.2}FeO_3$) and studied the WGS kinetics over that sample in the temperature range of 550-600 ^oC. They suggested that the power law type rate equation accurately fits the experimental results under the specified

operating conditions. For the temperature range of 550 – 600 ^{o}C, the reaction orders with respect to CO, H_2O, CO_2 and H_2 were found to be 0.81±0.02, -0.01±0.09, -0.22±0.02 and -0.039±0.002, respectively and the activation energy was reported as 86 kJ/mol.

Hakeem *et al*. (2015) comparatively studied the kinetics of the WGS reaction over three zirconia supported catalysts, (Fe_2O_3/ZrO_2, Rh/ZrO_2, and $Rh/Fe_2O_3/ZrO_2$) in the temperature range of 350-500 ^{o}C and at an operating pressure of 21 bar. They reported that the redox mechanism is the best fitting model for the Fe_2O_3/ZrO_2 catalyst and its activation energy (111 kJ.mol^{-1}) is greater than that of the Rh-based one (64 kJ.mol^{-1}). It was found that the presence of rhodium in $Rh/Fe_2O_3/ZrO_2$ makes the reaction rate constant five times higher than that of Rh/ZrO_2, but the activation energy value stays close to that of Fe_2O_3/ZrO_2. Also, upon the addition of rhodium to the Fe-based catalysts, the CO_2 inhibition becomes vital and the dependency on CO decreases, but that on H_2O increases.

The kinetic data for the low temperature WGS reaction over several copper-based catalysts (8%CuO-Al_2O_3, 8%CuO-15%CeO_2-Al_2O_3, 8%CuO-CeO_2 and 40%CuO-ZnO-Al_2O_3) were reported by Koryabkina *et al*. (2003) for the fuel cell applications at an operating temperature and a pressure of 200 ^{o}C and 1 atm, respectively. The dependencies on CO, H_2O, CO_2 and H_2 were found to be 0.8, 0.8, -0.9 and -0.9, respectively over the CuO-ZnO-Al_2O_3 sample for the forward reaction rate under the specified operating conditions. Moreover, authors determined that no promotion in WGS activity is observed upon the addition of either ceria or zinc oxide to the Cu-based catalysts, implying that the copper species are the only active phase for the target reaction. According to the results of this study, they proposed that the WGS reaction occurs through the redox mechanism with the rate-determining step of $CO* + O* \leftrightarrow CO_2* + *$.

2.3.2. Kinetics of Noble Metal-based WGS Catalysts

The development of novel noble metal-based catalysts with high activity, selectivity and stability for a single stage WGS reaction operating in the transition temperature range (between HTS and LTS) and a study on their kinetic behavior are important in the design and optimization of compact reactors for small-scale fuel processing/cell (FP-FC) applications.

The kinetic features of the low temperature WGS reaction over the Au/CeO_2 catalysts and the effect of active metal loading on the reaction rate were investigated by Leppelt *et al*. (2006) by testing 8 different gold-based catalysts with gold loadings changing between 0.8 and 12.6 wt%. The mechanism for the kinetic model was determined as the surface redox with the rate-determining step defined as the reduction of surface oxygen by adsorbed CO. Using the empirical power law type rate equation, the reaction orders of 0.5 for CO and H_2O and those of −0.5 for CO_2 and H_2 were estimated for the 2.6wt% Au loaded catalyst, which demonstrated the best performance among the catalysts investigated. However, for all the gold-based catalysts, the activation energy was evaluated as 40 kJ mol^{-1} in the temperature range of 80 – 180 ^oC. It was also revealed that the promoting effect of ceria in the catalysts is negligible on the reaction rate compared to Au species under the specified operating conditions.

At low operating temperatures (280–325 °C) and under the realistic feed conditions, the kinetic characteristics of the 1wt.%Au–0.5wt.%Re/CeO_2 catalyst was examined by Gökaliler *et al*. (2013) by changing the temperature and partial pressures of feed composition to the WGS reactor. They reported that the empirical power law type rate expression with the reaction orders of 0.75, 2.0, −0.34 and −0.60 for the feed components (CO, H_2O, CO_2 and H_2, respectively) partial pressures adequately fit the experimental data with an error margin of 10%. The apparent activation energy was estimated as 29.4 ± 0.400 kJ mol^{-1} in the temperature range of 280 – 325 ^oC.

In recent years, the application of platinum-based catalysts in small-scale fuel processors have attracted much attention. In this context, Phatak *et al*. (2007) studied kinetic parameters of the ceria and alumina supported Pt-based catalysts namely, 1wt.% Pt/CeO_2 and 1wt.% Pt/Al_2O_3 for the WGS reaction within a temperature range of 180–345 ^oC and at an atmospheric pressure. They observed that the ceria supported catalyst has a turnover frequency value 30 times as high as that of alumina supported one for the WGS reaction under the same operating conditions. The reaction orders evaluated for the Pt/Al_2O_3 sample were found to be 0.06, 1.0, -0.09 and -0.44 for CO, H_2O, CO_2 and H_2, respectively. Those over the Pt/CeO_2 catalyst were estimated as 0.1, 1.1, -0.07 and -0.44 for the same sequence of reaction components. In the temperature range of 225 – 285 ^oC,

the activation energy was evaluated as 75 kJ/mol for the ceria-based catalyst, while that for Pt/Al_2O_3 was found to be 84 kJ/mol.

In another kinetic study on a platinum-based catalyst (0.2 wt.% Pt loaded on CeO_2 support), Meunier *et al*. (2008) proposed that a negative order in terms of CO partial pressures can exist under certain operating conditions of the WGS reaction. They carried out the experiments at a temperature of 197 ^oC under 20% water and observed that an increase in the partial pressure of CO lead to a decrease in the reaction rate, implying that a negative order of CO can occur. Hence, at a temperature of 197 ^oC, the dependency on CO concentration was found to be -0.27. The results of this study confirmed the presence of the competitive adsorption between CO and H_2O molecules, which can have a significant effect in the WGS reaction mechanism.

The role of Re in the platinum-based catalysts, $Pt\text{-}Re/TiO_2$, was studied by Azzam *et al*. (2008) at 300 ^oC and 2 atm for the kinetics of WGS reaction. They reported that the partial presence of ReO_x in the $Pt–Re/TiO_2$ sample causes an additional redox route for the WGS reaction in such a way that ReO_x is reduced by CO to form CO_2 and then re-oxidized by water to produce hydrogen. The rate determining step was proposed as the reaction between CO adsorbed on platinum particles and OH groups adsorbed on TiO_2. The kinetic data were fitted to the empirical power-law type rate expression to determine the power values with respect to reaction components. It was determined that at higher CO concentrations, the rate was close to zero order in CO, but at lower CO concentrations, the reaction order of CO was estimated as 0.4. The reaction orders in terms of the partial pressures of H_2O, CO_2 and H_2 were estimated as 1, 0 and -0.5, respectively.

A similar study to the one above was carried out by Radhakrishnan *et al*. (2006), who examined the possible effect of a Re promoter on a Pt-based catalyst (2wt.% Pt-1wt./%$Re/CeO_2\text{-}ZrO_2$) under the WGS reaction conditions. In this study, the WGS kinetics of the Pt and Pt-Re species supported on an oxide mixture of ceria-zirconia were compared using the empirical power law rate model. As per the results of kinetic experiments, over the $Pt/CeO_2\text{-}ZrO_2$ sample, the dependencies on CO, H_2O, CO_2 and H_2 were evaluated as 0.07, 0.67, -0.16 and -0.57, respectively, whereas the orders for the same sequence of reaction components were found to be -0.05, 0.85, -0.05 and -0.32 over the $Pt\text{-}Re/CeO_2\text{-}$

ZrO_2 catalyst. The developed power law type expression proposed that an increase in the WGS reaction rate is mostly because of a larger power value for the water partial pressure and lower inhibitory effects of CO_2 and H_2 over Pt-Re/CeO_2-ZrO_2 compared to Pt/CeO_2-ZrO_2. For both catalysts, they calculated the activation energies as 17 kcal/mol in the temperature range of 210-240 $^{\circ}$C.

3. EXPERIMENTAL WORK

3.1. Materials

3.1.1. Chemicals

All the chemicals used in the catalyst preparation process are research grade as described in Table 3.1.

Table 3.1. Chemicals used for catalyst preparation

Chemicals	**Formula**	**Specification**	**Source**	**Molecular Weight (g/mol)**
Ammonium perrhenate	NH_4ReO_4	99.999%	Sigma-Aldrich	268.24
Cerium (III) nitrate hexahydrate	$Ce(NO_3)_3 \cdot 6H_2O$	99.99%	Sigma-Aldrich	434.23
Sodium carbonate	Na_2CO_3	99.9+%	Merck	105.99
Sodium nitrate	$NaNO_3$	99.0%	Carlo Erba Reagents	84.995
Tetraamine platinum (II) nitrate	$Pt(NH_3)_4(NO_3)_2$	99.995%	Aldrich	387.22
Titanium (IV) oxide	TiO_2	Anatase, 99.9%	Alfa Aesar	79.87
Water	H_2O	Deionized	-	18.02

3.1.2. Gases and Liquids

All gases used in this work were supplied by the Linde Group, Gebze, Turkey. The specifications and applications of the liquid and gases used for this study are given in Table 3.2. and 3.3 below.

Table 3.2. Specification and application of the liquid

Liquid	Formula	Specification	Application
Water	H_2O	Deionized	Aqueous solution, Reactant

Table 3.3. Specifications and applications of the gases

Gas	Formula	Specification	Application
Argon	Ar	99.995%	Inert, GC carrier gas
Carbon dioxide	CO_2	99.995%	Reactant
Carbon monoxide	CO	99.999%	Reactant
Dry air	N_2 & O_2 mixture	99.998%	GC 6-way pneumatic valve
Hydrogen	H_2	99.995%	Reactant, Reducing agent
Methane	CH_4	99.995%	Reactant

3.2. Experimental Systems

The experimental systems used in this study can be categorized as below.

- Catalyst Preparation System: This is used for the synthesis of support(s) and incipient-to-wetness impregnation process.

- Catalytic Reaction System: The system is made up of a feeding section which includes mass flow controllers, HPLC pump to deliver deionized water at a required flowrate and pressure and a mixing zone where the deionized water and feed gasses are mixed and heated prior to entering the reactor; a reaction section consisting of a ¼ inch stainless steel fixed-bed microreactor placed inside an electrically operated and temperature-controlled furnace.

- Product Analysis System: This mainly consists of a gas chromatographic analyzer used for detecting the composition of the product and feed streams during the product and feed analysis, respectively and operates in line with the catalytic reaction system.

3.2.1. Catalyst Preparation System

The incipient-to-wetness impregnation is a method applied in catalyst preparation process. The following equipment and devices: a Retsch UR1 ultrasonic mixer, a Büchner flask filled with support material, a KNF Neuberger vacuum pump, a Masterflex flowrate-controlled peristaltic pump and a beaker holding the precursor solution are the main parts of incipient wetness impregnation system (Figure 3.1). The deposition precipitation technique used in the support preparation for this study is illustrated in Figure 3.2. The system contains a Julabo ED-13 water bath, a 500ml beaker placed inside bath, a Heidolph RZR 2021 impeller to stir solution in beaker and a Mettler Toledo FE20 pH-meter.

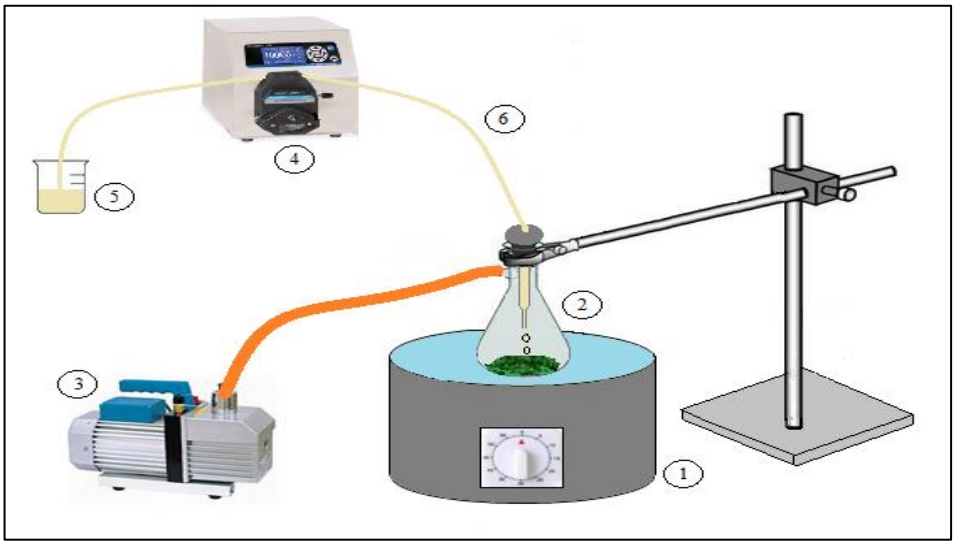

Figure 3.1. Schematic diagram of the incipient-to-wetness impregnation system: 1. Ultrasonic mixer, 2. Büchner flask, 3. Vacuum pump, 4. Peristaltic pump, 5. Beaker, 6. Silicone tubing (Başar, 2016).

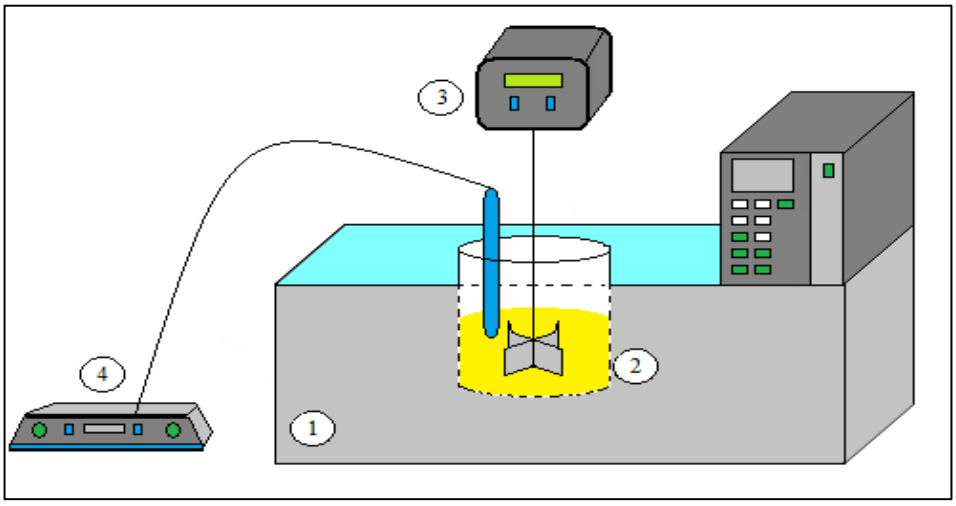

Figure 3.2. Schematic diagram of the deposition precipitation system: 1. Water bath, 2. Beaker, 3. Impeller, 4. pH-meter (Başar, 2016).

3.2.2. Catalytic Reaction System

For the current study, the water gas shift experiments were carried out in the catalytic reaction system which was designed and constructed in the Catalysis and Reaction Engineering Laboratory (CATREL) of Chemical Engineering Department at Boğaziçi University. The three main sections of the system – feed, reaction and product analysis are illustrated in Figure 3.3 below.

A group of mass flow controllers by Brooks Instrument to regulate the flowrate of various gases, an HPLC pump for water supply, 1/4'', 1/8'' and 1/16'' stainless steel tubing, valves and fittings make up the feed section. The gaseous reactants are kept in high-pressure cylinders and supplied to the reaction system at a pressure of 2.5 bar. From high-pressure cylinders up to the exit of mass flow controllers, each gas was supplied through a separate line to help determine the flowrate of the individual reactant. To avoid any possible back-pressure, an on-off valve was placed at the outlet stream of every mass flow controller. The three-way valve located prior to the reactor was used to direct the feed stream to the vent for about 1.5 hours in order to get a well-mixed gas mixture.

The deionized water in a liquid state was introduced to the reaction system at a controlled flowrate by an HPLC pumping system. To ensure that all water is completely vaporized before entering the reactor, the coiled 1/16" stainless steel tubes were heated up to 140±5 °C by a 104 W Cole-Parmer heating tape. The temperature of the 1/16" mixing/evaporating tubing was controlled by a Eurotherm 3216 PID controller connected to a K-type sheathed thermocouple. The mixing/evaporating line was also well insulated with ceramic wool to prevent heat loss to the surroundings.

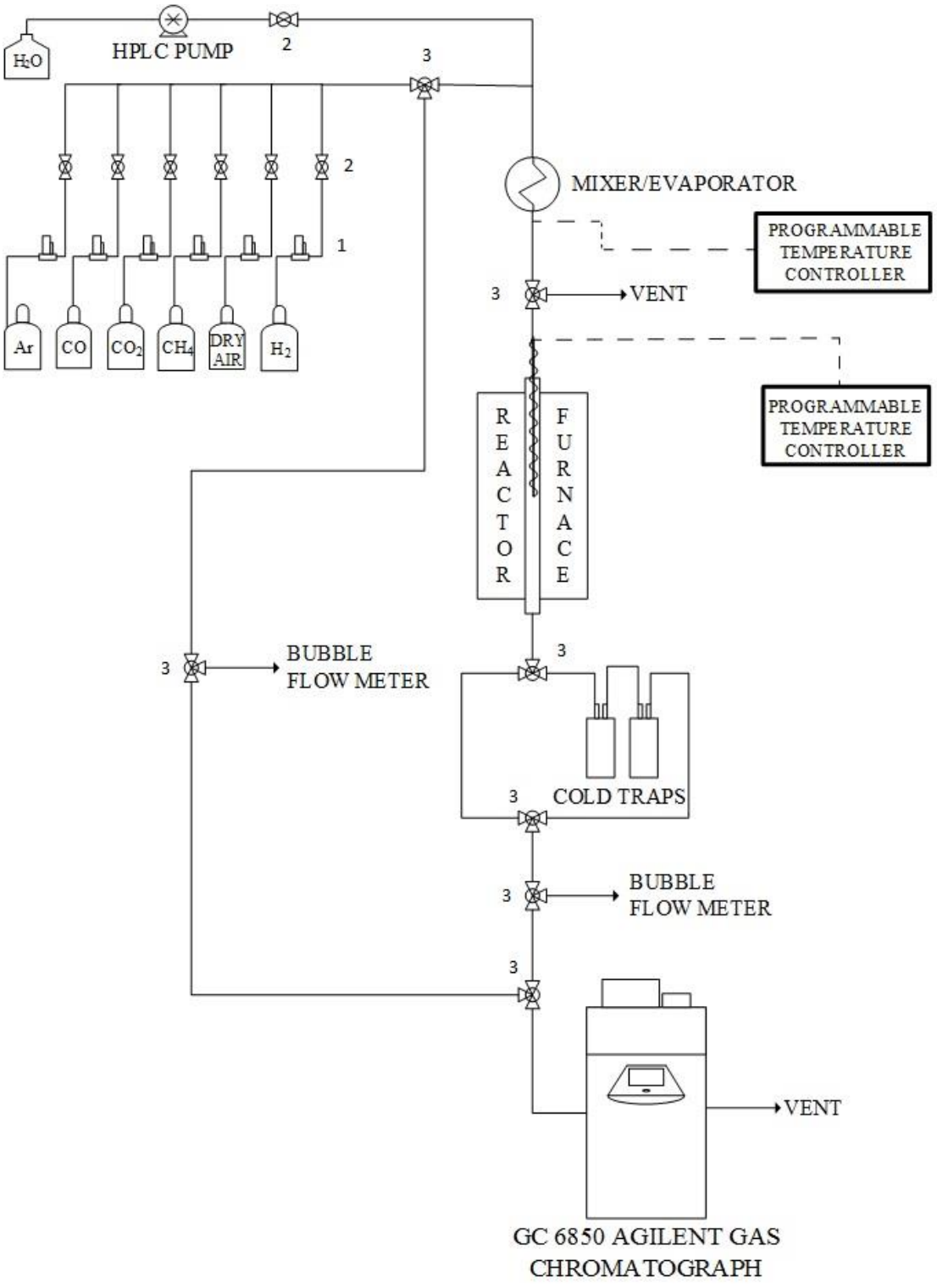

Figure 3.3. Schematic diagram of the catalytic reaction system:

1. Mass flow controller, 2. On-off valve, 3. Three-way valve (Demirhan, 2015).

After mixed for a sufficient time, the reactants were then introduced to the reaction section. The reaction system consists of a furnace with dimensions of 50 cm x 20 cm x 20 cm, a stainless-steel fixed bed microreactor with a length and an outside diameter of 71 cm and 1/4 inch, respectively and a Shimaden FP23 PID temperature controller connected to a K-type coated thermocouple. The microreactor was inserted inside the furnace and the silane treated glass wool was well packed at the center of the reactor to form a bed for the catalysts. The K-type sheathed thermocouple connected to a PID temperature controller was placed inside the furnace in such a way that it can measure the temperature of the catalyst bed. To maintain a stable temperature and avoid any possible heat loss, ceramic wool materials were used to insulate the top and bottom ends of the reactor. One of the reactants of WGS reaction, the unconverted or excess water steam can damage the gas chromatograph, if allowed to pass through the device. Therefore, a series of two condensers cooled down in an ice bed was placed at the exit of the reactor to remove water vapor from the reaction products. To prevent any possible blockage formed by condensed water in the tubing between the reactor exit and the ice bed, heat was supplied to that section of the system by a 104 W Cole-Parmer heating tape at a temperature of 140±5 °C.

3.2.3. Product Analysis System

An Agilent Technologies 6850 gas chromatograph (GC) equipped with a Hayesep D column and a thermal conductivity detector (TCD) was used for the analysis of gaseous feed and product compositions. The analysis conditions of the GC are defined in Table 3.4.

Prior to the experiments, the calibration of GC for gaseous reactants was carried out by injecting known volumes to find the peak areas corresponding to those volumes under the operating conditions given in Table 3.4. By linear regression technique, the volume percentage versus peak area curves was plotted for each gas and hence, the calibration factors were determined.

Table 3.4. Gas analysis conditions for the WGS reaction

GC Specifications	Agilent Technologies 6850
Detector type	TCD
Column temperature, °C	40
Inlet temperature, °C	100
Detector temperature, °C	150
Carrier gas	Argon
Carrier gas flow rate, ml/min	15
Column packing material	Hayesep D
Column tubing material	Stainless steel
Column length & ID	3m x 3 mm
Sample loop	1 ml

3.3. Catalyst Preparation and Pretreatment

In this study, Pt-Re-Na trimetallic systems supported on two different oxides (CeO_2 and TiO_2) were synthesized. The performance tests over the same catalysts were previously carried out by Eropak (2020) under the WGS reaction conditions.

The ceria (CeO_2) support was synthesized via homogeneous precipitation of cerium (III) nitrate hexahydrate ($Ce(NO_3)_3.6H_2O$) with the precipitation agent, sodium carbonate (Na_2CO_3). The Na_2CO_3 dissolved in deionized water was slowly added to the cerium precursor containing solution placed in a water bath at 60 ^oC and continuously stirred at 200 rpm as depicted in Figure 3.2. The sodium carbonate addition continued until the pH value of the solution was adjusted at 8. Then, the obtained suspension was left for 1 hour in a water bath at a controlled stirring speed, a temperature and a pH value of 200 rpm, 60 °C and 8, respectively. The resulting mixture was then filtered through a Watman filter paper and washed with deionized water for a few times under the application of vacuum. Lastly, it was left to dry overnight at 110 °C and calcined in a muffle furnace at 400 °C for 4 hours (Çağlayan, 2011).

Unlike the ceria support, TiO_2 was a commercial form as an anatase with 99.9% purity and was only calcined in a muffle furnace at 400 °C for 5 hours.

The trimetallic Pt-Re-Na/CeO_2 and Pt-Re-Na/TiO_2 catalysts, with 1wt.%Pt, 1wt.%Re, and 1wt.%Na, were prepared by a sequential impregnation method in such a way that Na, Re and Pt precursor solutions were consecutively added to the support materials as illustrated in Figure 3.1.

In the first step, the sodium nitrate ($NaNO_3$) dissolved in deionized water (1.25 ml deionized water for 1 gram of support) was added to the CeO_2 support via the incipient-to-wetness impregnation technique. 2 g of the CeO_2 support was placed in a Büchner flask and mixed by an ultrasonic mixer for approximately 25 minutes under vacuum in order to discharge the pores. The calculated amount of $NaNO_3$ solution was impregnated to the support material via a peristaltic pump at a flowrate of 0.5 ml/min. Then, the slurry-like substance was mixed ultrasonically for 1.5 h under vacuum and then left drying overnight at 110 °C. The next day, the dried slurry calcined for 2 h at 400 °C in a muffle furnace to get Na/CeO_2.

The Re-Na/CeO_2 catalyst was prepared by the impregnation technique, in which an aqueous solution of ammonium perrhenate (NH_4ReO_4) was added to calcined Na/CeO_2. The aqueous solution was prepared by dissolving a calculated amount of precursor in a definite amount of de-ionized water (1.25ml deionized water/g support). The Na/CeO_2 material was put in a Büchner flask and ultrasonically mixed for 25 minutes by applying vacuum. The NH_4ReO_4 solution was then added on the support through a peristaltic pump at a flowrate of 0.5 ml/min. The resulting slurry was left under vacuum and mixed ultrasonically for 1.5 h, dried overnight at 110 °C and then, calcined at 400 °C for 2 h in a muffle furnace next day.

Lastly, the calculated amount of the tetraamine platinum (II) nitrate ($Pt(NH_3)_4(NO_3)_2$) aqueous solution was added to Re-Na/CeO_2 via the incipient-to-wetness impregnation technique. The Re-Na impregnated CeO_2 support was put in a Büchner flask to be mixed in an ultrasonic mixer for 25 minutes under vacuum. The platinum precursor solution was impregnated on the support via a peristaltic pump at a flowrate of 0.5 ml/min.

The resulting slurry-like material was mixed ultrasonically for 1.5 h and then dried overnight at 110 °C. The dried slurry was calcined for 4h at 400 °C in a muffle furnace next morning.

For the preparation of 1%Pt-1%Re-1%Na/TiO_2 sample, 99.99% anatase (TiO_2) was used as a support material. Impregnation and calcination steps in the preparation procedure were followed in the same manner as were for the Pt-Re-Na/CeO_2 catalyst.

Before starting the experiments, the prepared samples were placed on the glass wool which was packed at the center of the microreactor. Pt-Re-Na/CeO_2 and Pt-Re-Na/TiO_2 catalysts were heated from the ambient temperature to the reduction temperature of 375 °C at a rate of 8.75 °C/min under the total flowrate of 100 ml/min containing 15% hydrogen with balanced amount of argon and reduced at 375 °C for 2 hours.

3.4. WGS Reaction Tests

3.4.1. Blank Tests

The intention in carrying out the blank tests was to guarantee that the materials of construction (i.e. stainless steel) and the silane treated glass wool have no catalytic activity.

3.4.2. WGS Performance Tests

The performance experiments for WGS reaction over the 1Pt-1Re-1Na/CeO_2 and 1Pt-1Re-1Na/TiO_2 samples were conducted by Eropak (2020) at 300, 350 and 400 °C for two realistic feed compositions given in Table 3.5. The experiments were carried out over 75 mg freshly reduced catalysts with 120,000 ml $gcat^{-1}h^{-1}$ GHSV for 6-hour TOS.

Table 3.5. Realistic feed compositions used for WGS performance tests

Feed	S/C	CO%	H_2O%	H_2%	CO_2%	Ar%
Realistic #1	6.7	4.9	32.7	30	10.4	22
Realistic #2	16.2	2.1	34.1	23.7	12.3	27.8

3.4.3. WGS Kinetic Tests

In order to derive the empirical power law type rate expressions for each of the 1Pt-1Re-1Na/CeO_2 and 1Pt-1Re-1Na/TiO_2 samples, the WGS kinetic experiments were carried out at different temperatures and partial pressures of CO, H_2O, H_2, CO_2 and CH_4 for two contact time, W/F over each sample. In the arrangement of the experimental sets for the kinetic study, the concentrations of CO, H_2O, H_2, CO_2 and CH_4 at 2, 45, 15, 10 and 7%, respectively were chosen as a reference experiment. As shown in Table 3.6, the kinetic tests were performed at three different partial pressures of each species (i.e. CO, H_2O, H_2, CO_2 and CH_4) for two different residence time values.

To estimate the activation energy, the reference experiment was repeated at 325 and 300 °C. The reactor was filled with 12 mg of a catalyst with the purpose of keeping the CO conversions at low values. The WGS kinetic experiments were performed in the reaction system described in Figure 3.3. Once the reduction process completed, the temperature of the catalyst bed was cooled from 375 ^oC down to the reaction temperature of 350 °C by allowing inert argon to flow through the reactor during the cooling process. When the temperature of catalyst bed stabilizes at 350 ^oC, inert gas was trapped inside the reactor and then, the reactants at their set values were diverted to the vent for 1.5 hour to obtain a steady state gas composition. The reaction initiated as soon as the reactants contacted the catalysts, which was observed by a slight increase in the temperature of the packed bed. The analysis of the product stream was performed at 0.25, 0.5, 1, 2 and 4 hours, while the feed analysis was conducted after the product analysis completed.

Table 3.6. Kinetic experiments performed over 1Pt-1Re-1Na/CeO_2 and 1Pt-1Re-1Na/TiO_2

Run #	**Total flow rate ($ml.min^{-1}$)**	**Percentage in feed stream (%)**						
		CO	**H_2O**	**H_2**	**CO_2**	**CH_4**	**Ar**	**H_2O/CO**
1	150	1	45	15	10	7	22	45
	200	1	45	15	10	7	22	45
2	150	2	45	15	10	7	21	22.5
	200	2	45	15	10	7	21	22.5
3	150	3	45	15	10	7	20	15
	200	3	45	15	10	7	20	15
4	150	2	60	15	10	7	6	30
	200	2	60	15	10	7	6	30
5	150	2	50	15	10	7	16	25
	200	2	50	15	10	7	16	25
6	150	2	30	15	10	7	36	15
	200	2	30	15	10	7	36	15
7	150	2	45	15	11	7	20	22.5
	200	2	45	15	11	7	20	22.5
8	150	2	45	15	9	7	22	22.5
	200	2	45	15	9	7	22	22.5
9	150	2	45	15	8	7	23	22.5
	200	2	45	15	8	7	23	22.5
10	150	2	45	18	10	7	18	22.5
	200	2	45	18	10	7	18	22.5
11	150	2	45	16	10	7	20	22.5
	200	2	45	16	10	7	20	22.5
12	150	2	45	12	10	7	24	22.5
	200	2	45	12	10	7	24	22.5

Table 3.6. Kinetic experiments performed over 1Pt-1Re-1Na/CeO_2 and 1Pt-1Re-1Na/TiO_2 (cont.)

Run #	Total flow rate ($ml.min^{-1}$)	Percentage in feed stream (%)						
		CO	H_2O	H_2	CO_2	CH_4	Ar	H_2O/CO
13	150	2	45	15	10	9	19	22.5
	200	2	45	15	10	9	19	22.5
14	150	2	45	15	10	8	20	22.5
	200	2	45	15	10	8	20	22.5
15	150	2	45	15	10	0	28	22.5
	200	2	45	15	10	0	28	22.5

The kinetics of WGS reaction at different temperatures and feed compositions can be described by an empirical power law type model (Equation 3.1) for various metal-based catalysts.

$$-r_{CO} = k\, P_{CO}^{\alpha}\, P_{H2O}^{\beta}\, P_{CO2}^{\gamma}\, P_{H2}^{\delta}\, P_{CH4}^{\theta}(1-\beta') \tag{3.1}$$

where, the β' parameter is the factor of reversibility and can be calculated as:

$$(1-\beta') = \left(1 - \frac{1}{K_{eq}} \frac{P_{H_2} P_{CO_2}}{P_{CO} P_{H_2O}}\right) \tag{3.2}$$

The higher the β' value, the higher the reverse WGS reaction rate. Therefore, the β' value should be less than 0.1 for the application of the method of initial reaction rates.

4. RESULTS AND DISCUSSION

New non-intermittent power technologies having potential to alleviate demand on fossil fuels and to mitigate greenhouse gas emissions and air pollution are expected to become well-proliferated soon. In this sense, the bio-hydrocarbons fueled fuel processors operating in line with the proton exchange membrane fuel cells (FP-PEMFC) used for small-scale stationary electricity production can be considered as a promising option for the steady energy supply. Among other fuel cells available in markets, a hydrogen fueled PEMFC is considered as the most favorable one due to its high efficiency with negligible/no emissions, low maintenance cost and silent operation (Eropak and Aksoylu, 2017; Moreno *et al*, 2008).

Since hydrogen still has technological hurdles in its storage and distribution, on-site hydrogen production through using an FP from hydrocarbons having well-established distribution systems can be considered as an alternative to hydrogen storage. In a typical FP, three catalytic processes, the reforming of hydrocarbons, water gas shift (WGS) and preferential CO oxidation (PROX) reactions are conducted in series. The gas mixture rich in H_2, produced via the reforming reaction, also contains some amount of CO, which is the potential poison for Pt-based electro-catalysts of PEMFCs. Therefore, in order to protect electrodes from poisoning, CO concentration in the reformate stream needs to be lowered down to 100 ppm or below prior to entering the PEMFC. The CO clean-up process is generally performed by the WGS unit followed by a final CO removal step – PROX reactor (Koroneos *et al*, 2004; Ercolino *et al*, 2015).

Focusing on the intermediate WGS unit of a typical fuel processor, the current study aimed to determine the empirical power-law type kinetic expressions for the WGS reaction over the Pt-Re-Na trimetallic systems having the same metal loadings, but synthesized on different supports, CeO_2 and TiO_2. The current work also studied the effect of methane presence in the feed stream on the kinetics of the target reaction under realistic conditions. The oxidative steam reforming (OSR) product composition experimentally determined by Başar (2016) was used as the reference realistic feed for the WGS reaction.

The results of this study are important in the sense that they can be practically used in designing, optimizing and controlling a typical FP producing PEMFC-grade hydrogen.

The results of this work are summarized in 3 sections. The first part presents and discusses the results of WGS performance tests carried out by Eropak (2020). The preliminary kinetic tests over 1Pt-1Re-1Na/CeO_2 and 1Pt-1Re-1Na/TiO_2 conducted to determine the optimum values for temperature, steam to carbon ratio (H_2O/CO) and residence time as well as the reaction conditions guaranteeing kinetically controlled and mass transfer limitation free zone are given in the second section. The third and final part discusses the results of kinetic experiments and presents the power-law type kinetic expressions for the WGS reaction over both Pt-based trimetallic catalysts.

4.1. A summary of WGS Performance Test Results (Eropak, B.M., 2020)

Previously, our group (Eropak, B.M., 2020) carried out the WGS performance experiments over both samples (1Pt-1Re-1Na/CeO_2 and 1Pt-1Re-1Na/TiO_2) under realistic feed conditions. The tests were performed at 300, 350 and 400 °C under realistic feed #1 (H_2O/CO of 6.7) and realistic feed #2 (H_2O/CO of 16.2) conditions as shown in Table 3.5. The experiments were conducted at a pressure and a constant GHSV of 1 atm and 120,000 ml $gcat^{-1}$ h^{-1}, respectively, and 75 mg of freshly reduced catalyst was used in each WGS performance test. The difference in catalytic activity under different operating conditions was observed by comparing CO conversion values at the end of 2 h time on stream (TOS). The calculation of CO conversion was performed as per Equation 4.1 below.

$$\text{CO conversion (\%)} = \left(\frac{f_{\text{CO,in}} - f_{\text{CO,out}}}{f_{\text{CO,in}}}\right) \times 100 \qquad (4.1)$$

where $f_{CO,in}$ and $f_{CO,out}$ are the reactor inlet and outlet molar flowrate of carbon monoxide. The stability of catalysts was determined by measuring the loss in activity over 6 h TOS as defined in Equation 4.2.

$$\text{Activity loss (\%)} = \left(\frac{[\text{CO conversion}]_{0.5\text{h}} - [\text{CO conversion}]_{6\text{h}}}{[\text{CO conversion}]_{0.5\text{h}}}\right) \times 100 \qquad (4.2)$$

The activity losses observed under realistic feed #1 conditions for the 1Pt-1Re-1Na/CeO_2 and 1Pt-1Re-1Na/TiO_2 samples are presented in Figure 4.1 and 4.2. While the activity losses for 1Pt-1Re-1Na/CeO_2 in 6 h TOS period were calculated as 3.8%, 4.2% and 2.4%, those for the 1Pt-1Re-1Na/TiO_2 catalyst were found to be as 1.1%, 0.2% and ~0% at temperatures of 350 °C, 400 °C and 300 °C, respectively.

The stability tests were also performed under realistic feed #2 conditions for both catalysts and the results are illustrated in Figure 4.3 and 4.4. The activity losses for 1Pt-1Re-1Na/CeO_2 in 6 h TOS period were calculated as 3.8%, 4.2% and 2.4%, while those over the 1Pt-1Re-1Na/TiO_2 catalyst were calculated as 1.1%, 0.2% and ~0% at temperatures of 350 °C, 400 °C and 300 °C, respectively.

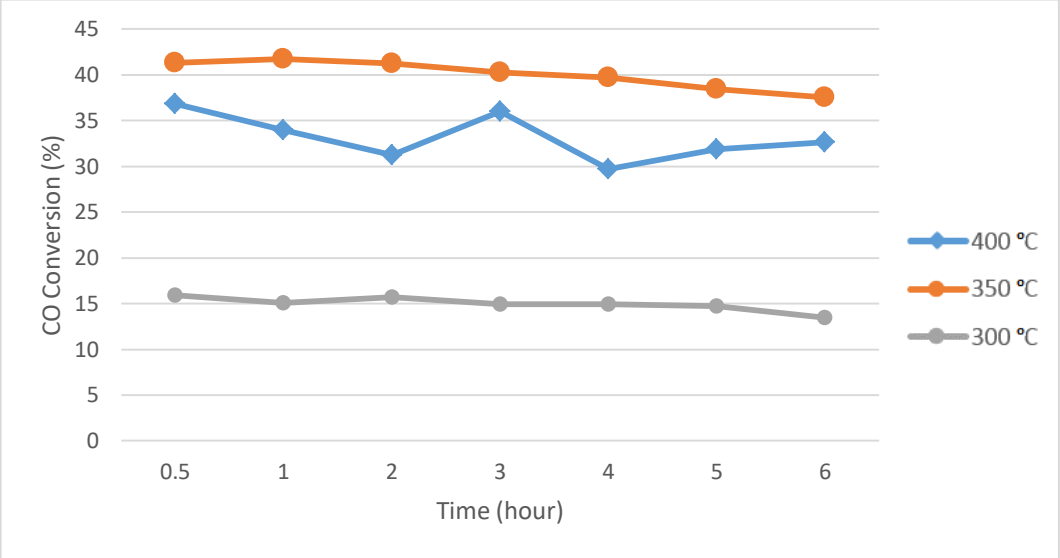

Figure 4.1. Activity tests over 1Pt-1Re-1Na/CeO_2 for real feed #1 at different temperatures

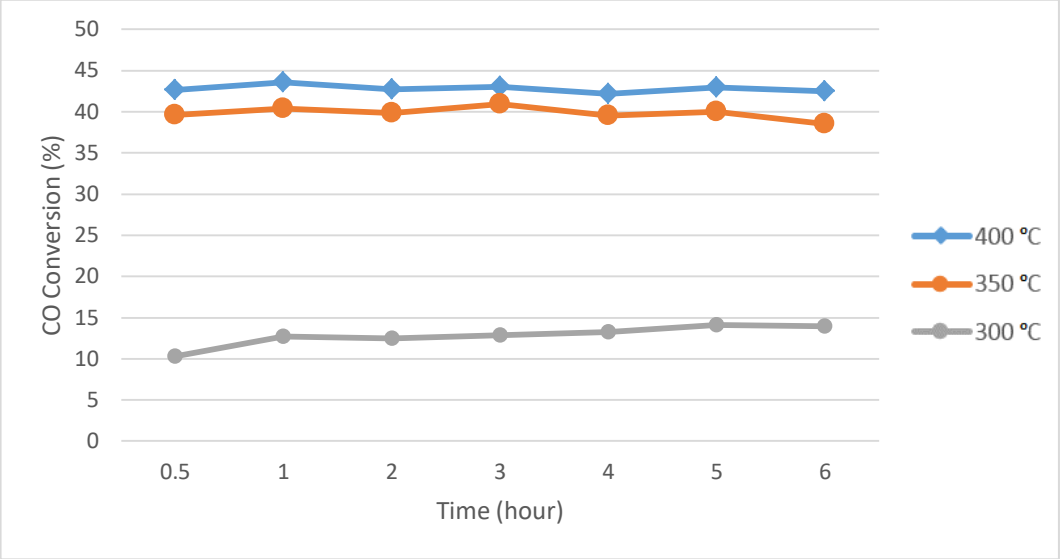

Figure 4.2. Activity tests over 1Pt-1Re-1Na/TiO_2 for real feed #1 at different temperatures.

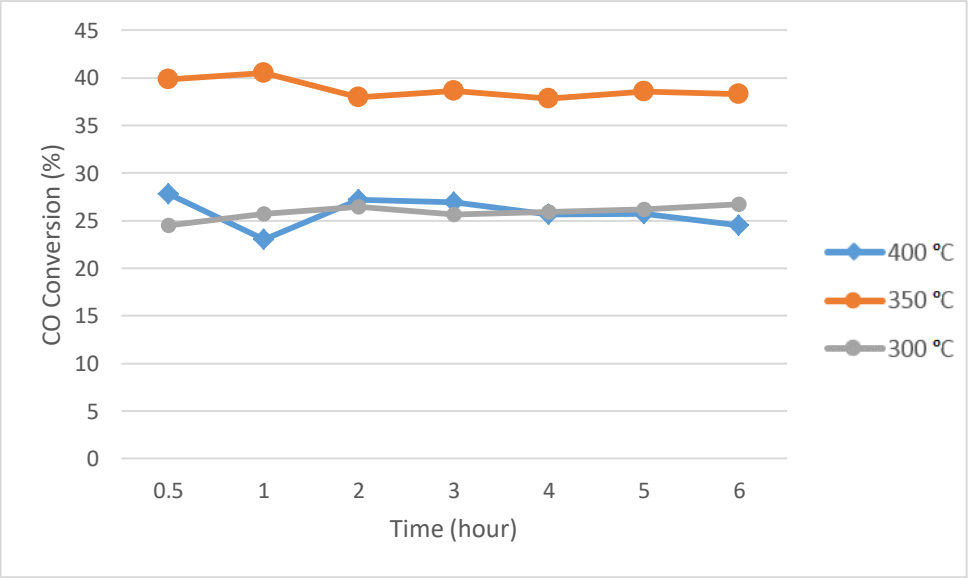

Figure 4.3. Activity tests over 1Pt-1Re-1Na/CeO_2 for real feed #2 at different temperatures

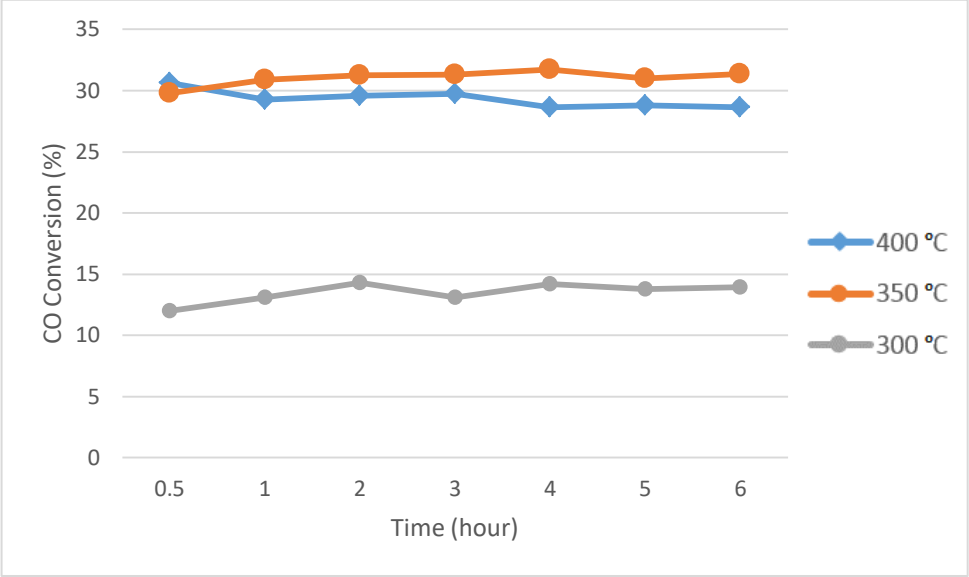

Figure 4.4. Activity tests over 1Pt-1Re-1Na/TiO_2 for real feed #2 at different temperatures

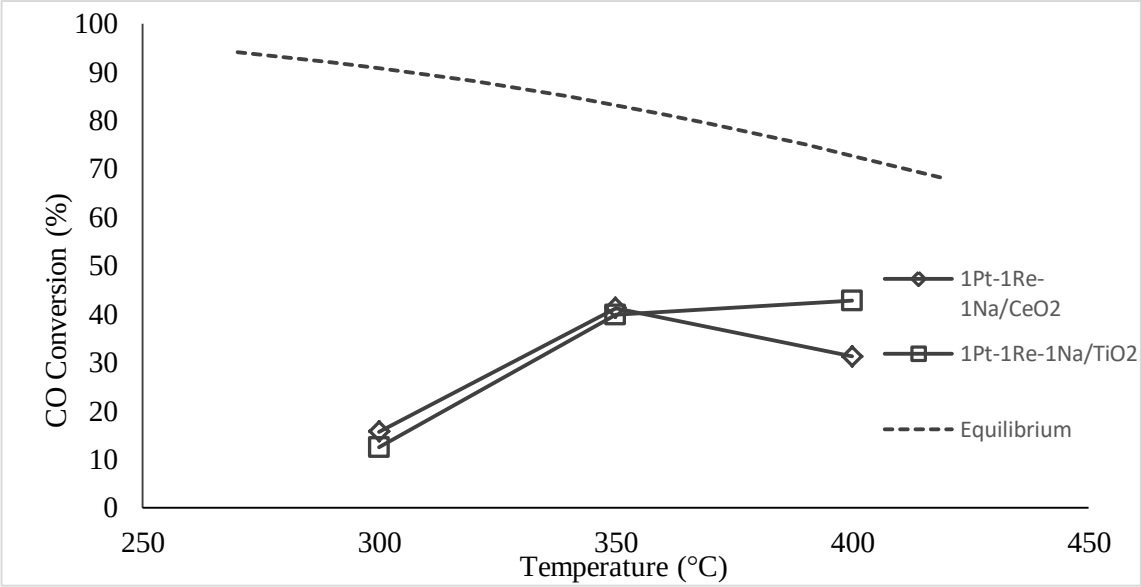

Figure 4.5. Temperature dependency of catalytic activity under real feed #1 conditions

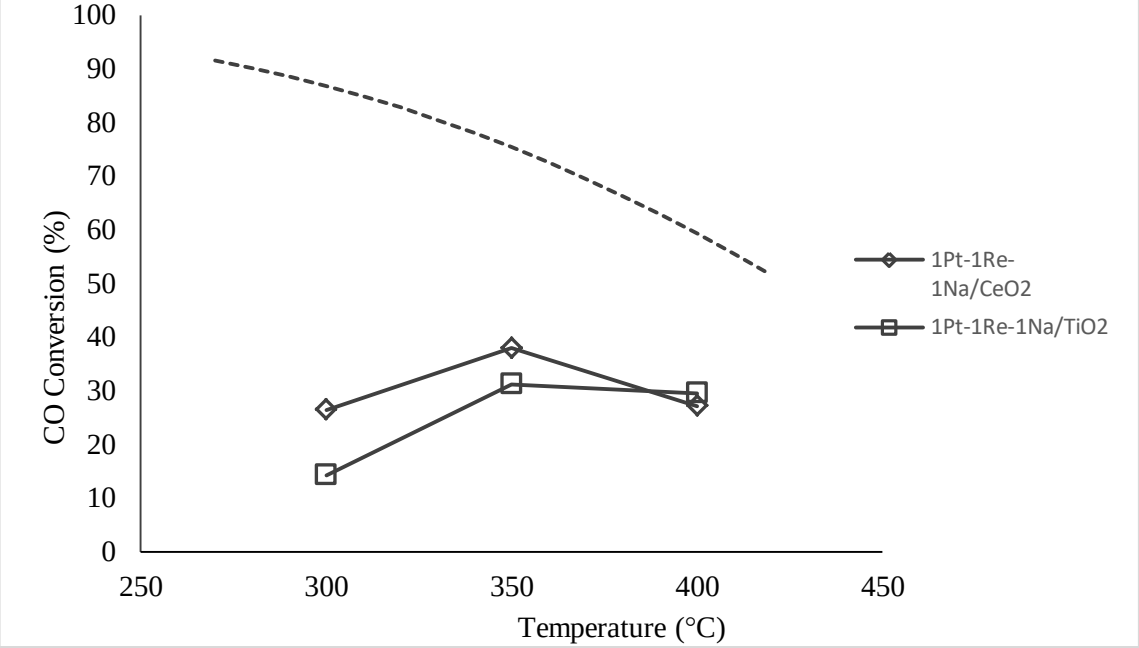

Figure 4.6. Temperature dependency of catalytic activity under real feed #2 conditions

Under realistic feed #1 and realistic feed #2 conditions, the CO conversions at three different temperatures (300, 350 and 400 ^{o}C) were plotted against their respective operating temperatures to understand the effect of temperature on the catalytic activity. Figure 4.5 illustrates the conversion dependency on temperature for S/C ratio of 6.7, while Figure 4.6 plots conversion against temperature for S/C ratio of 16.2. Under the same feed conditions, the equilibrium CO conversions were plotted with the help of HSC-Chemistry Software.

Under both realistic feed #1 and realistic feed #2 conditions, an increase in the operating temperature up to 350 °C promotes the WGS activity of the 1Pt-1Re-1Na/CeO_2 sample. However, a further increase in temperature (above 350 °C) leads to a reduction in the catalytic performance of this catalyst. In this trend, 1Pt-1Re-1Na/CeO_2 showed its highest activity for realistic feed #1 at 350 °C with 41.24% CO conversion while the equilibrium conversion value was calculated as 83.18%. This catalyst reached 37.98% conversion value corresponding to thermodynamic equilibrium conversion of 75.42% under realistic feed #2 conditions.

The WGS performance of 1Pt-1Re-1Na/TiO_2 under realistic feed #1 conditions showed slightly different trend from that of 1Pt-1Re-1Na/CeO_2 in a way that 1Pt-1Re-1Na/TiO_2 reached its highest conversion value of 42.75% at 400 ^oC while 39.81% conversion was achieved at 350 ^oC. However, under realistic feed #2 conditions, the best performance was observed at 350 ^oC, at which the 1Pt-1Re-1Na/TiO_2 catalyst converts 31.24% of CO compared to 29.58% conversion obtained at 400 ^oC.

As it is intended to enrich hydrogen concentration along with CO reduction through the WGS reaction, a catalyst used for the target reaction must be selective towards H_2 and able to prevent the unwanted methanation reaction which consumes hydrogen. According to Eropak's (2020) study, during the WGS reaction over the 1Pt-1Re-1Na/CeO_2 and 1Pt-1Re-1Na/TiO_2 samples no methanation occurred under different operating conditions investigated. Therefore, being highly active, stable for long time and selective towards desirable products, the 1Pt-1Re-1Na/CeO_2 and 1Pt-1Re-1Na/TiO_2 catalysts are practical for WGS reaction of FP systems.

4.2. Kinetic Preliminary Tests of WGS Reaction

The preliminary kinetic tests were conducted with the intention of determining experimental parameters guarantying the WGS reactions carried out in a kinetically controlled and mass-transfer limitation free zone. To do so, carbon monoxide conversions were minimized as much as possible within the realistic operating conditions.

According to a previous study performed by our group member (Eropak, 2020), an operating temperature of 350 ^oC resulted in the highest catalytic activity over the samples investigated, suggesting the kinetic tests should be carried out at that temperature. Unlike WGS performance experiments, 12 mg of catalysts (instead of 75 mg used in the performance tests) was used to lower CO conversions and hence, ensure that the experiments were performed in a kinetically controlled zone. Before the preliminary kinetic tests, blank experiments were conducted with a glass wool packed reactor just to guarantee that neither the material of construction (i.e. stainless steel) nor the glass wool was catalytically active under the specified operating conditions. Moreover, two different values for the contact/residence time (W_{cat}/F_{CO}) were selected through altering the total

flowrate between 150 and 200 mL/min and keeping the catalyst load constant, to get a linear relationship between the CO conversion and W_{cat}/F_{CO}. Two different values chosen for the residence time corresponded to gas hourly space velocities (GHSV) of 0.75×10^6 and 1×10^6 ml $gcat^{-1}$ h^{-1}, at total flowrates of 150 and 200 mL/min respectively.

In a typical fuel processor, OSR product is fed to WGS reactor. Accordingly, the reference WGS feed composition was specified based on a previous experimental study performed by our group (Başar, 2016), in which product distribution of propane OSR reaction was determined over the Pt-Ni/Al_2O_3 catalyst. The realistic feed composition for the present kinetic study was determined through considering the product composition range obtained in OSR performance tests conducted for S/C feed ratios of 3 and 6 at temperature of 350 °C (Başar, 2016); the mean values of those product compositions were calculated and presented in Table 4.1.

Table 4.1. Propane OSR product distribution determined via the OSR experiments performed at 350 °C for S/C feed ratios of 3 and 6 (Başar, 2016)

		Wet Based Product Concentration (%)							
T_{OSR} (^oC)	**S/C**	H_2	CO	CH_4	CO_2	C_3H_8	O_2	H_2O	He
350	2.25	9.3	0.18	11.8	10.5	0.047	0.004	40.3	28.0
350	3.00	10.6	0.28	10.3	10.9	0.005	0.004	43.7	24.2
350	5.00	10.1	0.26	7.2	8.3	0.136	0.004	56.5	17.5
350	6.00	9.5	0.28	6.4	7.0	0.249	0.003	61.3	15.4

As listed in Table 3.6, the feed composition in Run #1 of kinetic experiments was compatible with the product distribution of OSR reaction, but the reference kinetic test was chosen as Run #2 due to the fact that the value signifying the proximity to equilibrium (β') for WGS was greater than 0.1 under Run 1 conditions, indicating that the WGS reaction was performed near the equilibrium region rather than the initial rate zone. The inhibitory effect of hydrogen and carbon dioxide on the forward reaction was relatively higher under Run #1 conditions, which is an unwanted case for kinetic tests.

The reference experiments (Run #2 in Table 3.6) were carried out over the 12 mg freshly reduced 1Pt-1Re-Na/CeO_2 and 1Pt-1Re-1Na/TiO_2 samples at 350 °C and total flow rates of 150 and 200 ml/min. Based on R^2 values it was confirmed that the experiments were performed in a kinetically controlled region as depicted in Figure 4.7 below.

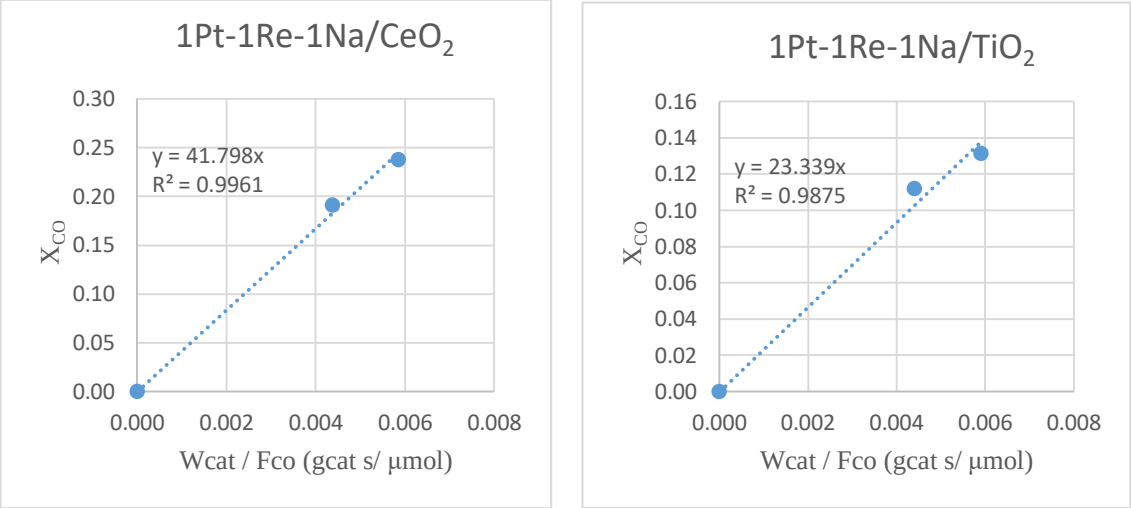

Figure 4.7. Graphs of CO conversion vs residence time for Run #2 over the 1Pt-1Re-Na/CeO_2 and 1Pt-1Re-1Na/TiO_2 catalysts

4.3. The WGS Kinetic Tests

Using different feed compositions given in Table 3.6, 15 sets of kinetic experiments were carried out at 350 °C and an atmospheric pressure. To balance the total flowrates at specified values (i.e. 150 or 200 ml/min), argon as an inert gas was introduced to the reaction system. The steam to carbon (H_2O/CO) ratio was maintained between 15 and 45 by altering the water and carbon monoxide concentrations accordingly. The relationship between the reaction rate and the partial pressures of CO, H_2O, H_2, CO_2 and CH_4 was determined using an empirical power law type model. By altering the total flowrate between 150 and 200 ml/min and keeping the catalyst load constant at 12 mg, various residence time values were obtained to calculate the initial reaction rate ($-r_{CO}$) shown in Equation 4.3 for each set of the kinetic tests.

$$-r_{CO} = \frac{dX_{CO}}{d(W_{cat}/F_{CO})} \tag{4.3}$$

where $-r_{CO}$, X_{CO}, W_{cat} and F_{CO} are the reaction rate in μmol g^{-1} s^{-1}, the conversion of carbon monoxide, the weight of catalyst in g and the flowrate of carbon monoxide μmols^{-1}, respectively.

In the graphs of the CO conversion plotted against residence time (see Appendix A), the slopes of the straight lines drawn give the initial reaction rates as listed in Table 4.2 and 4.3. The dependency of the reaction rate on the feed components (CO, H_2O, H_2, CO_2 and CH_4) was determined by using the power-law type rate expression as shown in Equation 4.4.

$$-r_{CO} = [k_0 e^{(-\frac{E_A}{RT})}] P_{CO}^{\alpha} P_{H_2O}^{\beta} P_{H_2}^{\delta} P_{CO_2}^{\gamma} P_{CH_4}^{\varepsilon} (1 - \beta') \tag{4.4}$$

where α, β, δ, γ and ε are the power values, k_0, E_A, R, T and P are the pre-exponential factor, activation energy in kJ mol^{-1}, universal gas constant in kJ mol^{-1} K^{-1}, temperature in K and partial pressure of each component in kPa, respectively. The closeness to equilibrium is defined by β' which can be calculated using Equation 4.5.

$$\beta' = \frac{1}{K_{eq}} \frac{P_{H_2} P_{CO_2}}{P_{CO} P_{H_2O}} \tag{4.5}$$

The equilibrium constant (K_{eq}) was estimated as 20.45 at an operating temperature of 350 °C according to Equation 4.6 below.

$$K_{eq} = \exp\left(\frac{4577.8}{T} - 4.33\right) \tag{4.6}$$

The reaction orders (α, β, δ, γ and ε) were evaluated by taking natural logarithm of Equation 4.4 and applying linear regression to it.

$$\ln(-r_{CO}) = lnk + \alpha \ln(P_{CO}) + \beta \ln(P_{H_2O}) + \delta \ln(P_{H_2}) + \gamma \ln(P_{CO_2}) + \varepsilon ln(P_{CH_4}) \quad (4.7)$$

The results of 30 experiments, for which 3 different values for the partial pressures of each component [(CO, H_2O, H_2, CO_2 and CH_4)] and 2 different values for the residence time (W_{cat}/F_{CO}) conducted, as 15 pairs, for each catalyst were used to determine the effect of partial pressures on the reaction rate. The concentration of CH_4 was kept fixed in 12 pairs of kinetic tests, while it was altered in the remaining 3 pairs to observe the dependency of reaction rates on methane. The partial pressure of each component, the experimentally determined reaction rates and the values for the closeness to equilibrium (1-β') and R^2 were calculated for 1Pt-1Re-1Na/CeO_2 and 1Pt-1Re-1Na/TiO_2 samples at a temperature of 350 ^oC are all listed in Table 4.2 and 4.3.

Table 4.2. Feed compositions and calculated initial reaction rates over 1Pt-1Re-1Na/CeO_2 at 350 °C

	Partial Pressures (kPa)							
	CO	**H_2O**	**H_2**	**CO_2**	**CH_4**	**Reaction Rate (µmol/ g_{cat} s)**	**(1-β')**	**R^2**
Run #1	1.01	45.60	15.20	10.13	7.09	22.011	0.837	0.9973
Run #2	2.03	45.60	15.20	10.13	7.09	41.798	0.919	0.9961
Run #3	3.04	45.60	15.20	10.13	7.09	58.504	0.946	0.9669
Run #4	2.03	60.80	15.20	10.13	7.09	49.774	0.939	0.9999
Run #5	2.03	50.66	15.20	10.13	7.09	43.432	0.927	1.0000
Run #6	2.03	30.40	15.20	10.13	7.09	38.602	0.878	0.9937
Run #7	2.03	45.60	15.20	11.15	7.09	39.271	0.910	0.9626
Run #8	2.03	45.60	15.20	9.12	7.09	44.825	0.927	0.9945
Run #9	2.03	45.60	15.20	8.11	7.09	45.438	0.935	0.9829
Run #10	2.03	45.60	18.24	10.13	7.09	40.090	0.902	0.9633
Run #11	2.03	45.60	16.21	10.13	7.09	42.725	0.913	0.9949
Run #12	2.03	45.60	12.16	10.13	7.09	47.185	0.935	0.9889
Run #13	2.03	45.60	15.20	10.13	9.12	42.426	0.919	0.9979
Run #14	2.03	45.60	15.20	10.13	8.11	42.742	0.919	0.9798
Run #15	2.03	45.60	15.20	10.13	0.00	44.495	0.919	0.9991

Table 4.3. Feed compositions and calculated initial reaction rates over 1Pt-1Re-1Na/TiO_2 at 350 °C

	Partial Pressures (kPa)							
	CO	**H_2O**	**H_2**	**CO_2**	**CH_4**	**Reaction Rate (μmol/ g_{cat} s)**	**(1-β')**	**R^2**
Run #1	1.01	45.60	15.20	10.13	7.09	13.048	0.837	0.9917
Run #2	2.03	45.60	15.20	10.13	7.09	23.339	0.919	0.9875
Run #3	3.04	45.60	15.20	10.13	7.09	26.826	0.946	0.9822
Run #4	2.03	60.80	15.20	10.13	7.09	28.441	0.939	0.9984
Run #5	2.03	50.66	15.20	10.13	7.09	24.006	0.927	0.9865
Run #6	2.03	30.40	15.20	10.13	7.09	18.962	0.878	0.9973
Run #7	2.03	45.60	15.20	11.15	7.09	22.733	0.910	0.9979
Run #8	2.03	45.60	15.20	9.12	7.09	23.774	0.927	0.9974
Run #9	2.03	45.60	15.20	8.11	7.09	24.889	0.935	0.9987
Run #10	2.03	45.60	18.24	10.13	7.09	20.638	0.902	0.9993
Run #11	2.03	45.60	16.21	10.13	7.09	21.686	0.913	0.9729
Run #12	2.03	45.60	12.16	10.13	7.09	24.121	0.935	0.9990
Run #13	2.03	45.60	15.20	10.13	9.12	21.342	0.919	0.9960
Run #14	2.03	45.60	15.20	10.13	8.11	21.184	0.919	0.9980
Run #15	2.03	45.60	15.20	10.13	0.00	21.668	0.919	0.9965

Under the specified operating conditions, the reverse-WGS reaction can be considered negligible for cases where β' values are less than 0.1; it should be noted that β' is less than 1 in 13 pairs of kinetic experiments except Run #1 (β'=0.163) and #6 (β'=0.122) which slightly exceeds that limit. As summarized in Table 4.4, the reaction orders in the power law type rate expression (Equation 4.4) were evaluated for both catalysts via using the non-linear multivariable optimization analysis in MATLAB™ environment.

As seen in Table 4.2 and 4.3, a rise in the concentrations of CO and H_2O had a positive effect on the developed power law type rate expressions, while that in H_2 and CO_2 partial pressures lead to a decrease in the forward reaction rate. The role of methane in the proposed empirical rate expressions was also analyzed by varying its partial pressure, but no change in the experimental reaction rate was observed. This finding were supported further by no change in the reaction order for each component (α, β, δ, γ, ε) in presence and absence of methane.

Table 4.4. WGS reaction orders over 1Pt-1Re-1Na/CeO_2 and 1Pt-1Re-1Na/TiO_2

Catalyst Formula	**α**	**β**	**δ**	**γ**	**ε**
1Pt-1Re-1Na/CeO_2	0.79	0.24	-0.30	-0.31	-0.0018
1Pt-1Re-1Na/TiO_2	0.57	0.45	-0.30	-0.32	0.0015

In order to visualize the effect of CH_4 partial pressure on the reaction rate obtained over both catalysts (1Pt-1Re-1Na/CeO_2 and 1Pt-1Re-1Na/TiO_2), 3 pairs of experiments were carried out and the subsequent results are presented in Figure 4.8 and 4.9. It can be observed that a change in methane concentration has a negligible effect on CO conversion.

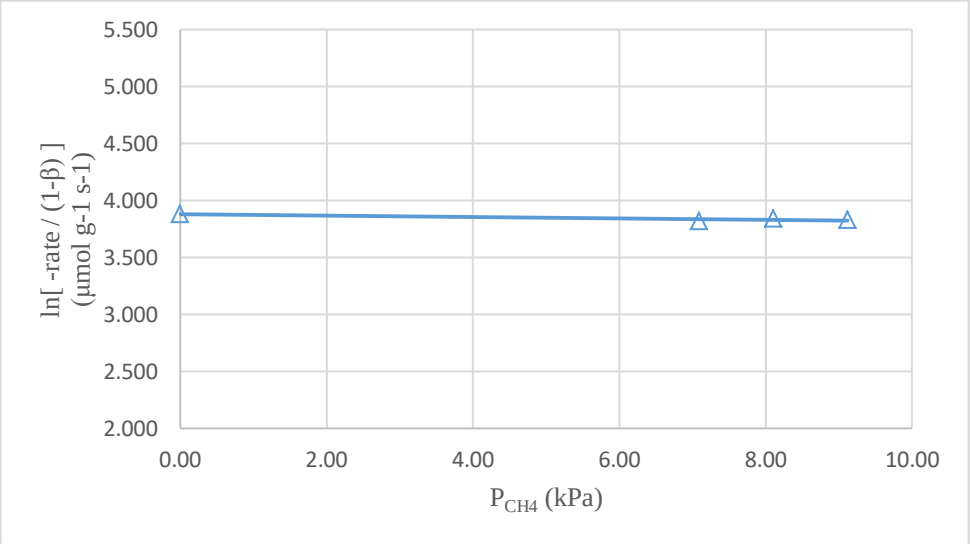

Figure 4.8. The effect of CH_4 partial pressure on the WGS reaction rate over 1Pt-1Re-1Na/CeO_2

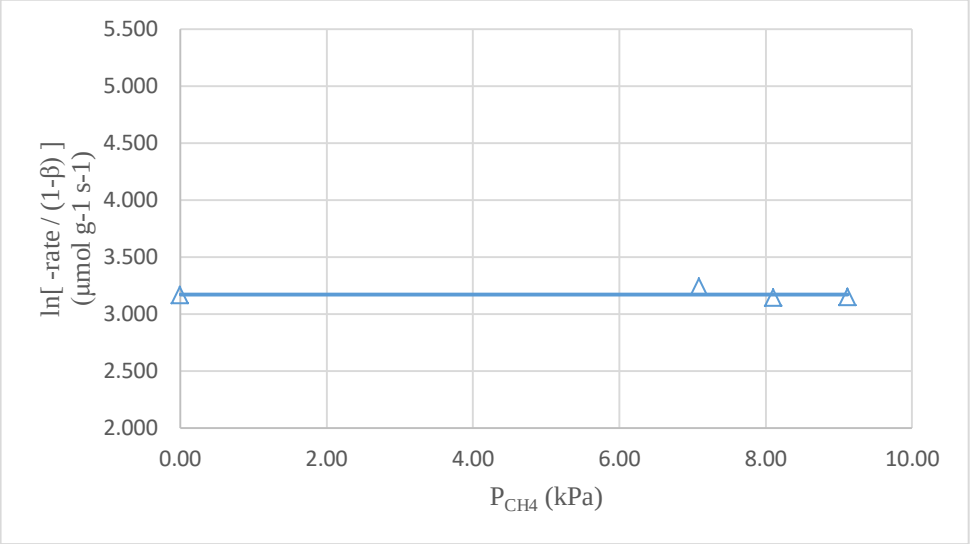

Figure 4.9. The effect of CH_4 partial pressure on the WGS reaction rate over 1Pt-1Re-1NaTiO_2

Since the operating conditions used for several studies on WGS kinetics are different, making one-to-one comparison between the reaction orders obtained in this study and those published in the literature for the noble metal-based catalysts would not be healthy. In previously published WGS kinetic studies, the reaction rate dependency on CO in the power-law type rate expressions was nearly zero at high CO partial pressures, while a positive order was obtained for CO at low carbon monoxide concentrations (Phatak *et al.*, 2007; Azzam *et al.*, 2008). This was explained by the phenomenon that the surface saturation of active metals by adsorbed CO molecules has a negative effect on the reaction rates (Phatak et al., 2007) In the present work, the WGS reaction was carried out at low carbon monoxide concentrations and at a medium operating temperature (350 ^{o}C), making the comparison reasonable with those performed over the Pt-based catalysts under similar operating conditions (Kalamaras *et al.*, 2009; Thinon *et al.*, 2009; Yumru, 2017).

Although the catalyst compositions and metal loadings are different, the results obtained for both samples in the current work are in a good agreement with those previously reported by our group under analogous operating conditions (Yumru, 2017). According to the WGS kinetic study conducted by Yumru (2017), the reaction orders in terms of CO, H_2O, CO_2 and H_2 over the 1Pt-0.5Re-1V/CeO_2 catalyst were found as 0.82, 0.31, -0.29 and -0.35, respectively, which are compatible with those found in current study.

The reaction orders for species involved in WGS reaction (CO, H_2O, CO_2 and H_2) over two different platinum-based catalysts, 1Pt/CeO_2 and 1Pt/TiO_2, were proposed over a wide range of CO concentrations (0-20%) by Thinon *et al*. (2009). Similar to the current study, the promoting effect of CO and H_2O and the inhibiting effect of CO_2 and H_2 on the proposed reaction rate over 1Pt/CeO_2 and 1Pt/TiO_2 samples were mentioned. In their study, the reaction orders of 0.14±0.04, 0.66±0.14, -0.08±0.03, and -0.54±0.03 over 1wt.%Pt/CeO_2 and 0.30±0.05, 0.85±0.10, 0±0.03, and -0.67±0.03 over 1wt.%Pt/TiO_2 were reported for the sequence of CO, H_2O, CO_2 and H_2.

The revealed inhibitory effect of CO_2 and H_2 on the forward WGS reaction rate in the current work was previously mentioned by Phatak *et al*. (2007), who reported the dependencies on CO_2 and H_2 as -0.1 and -0.38, respectively under the operating conditions relevant to fuel processing for fuel cell applications. In the literature, the negative reaction order for H_2 was explained by the presence of competitive adsorption between hydrogen and carbon monoxide molecules (Kalamaras *et al*. 2009). However, in an alternative explanation by Azzam *et al*. (2008), inhibitory effect of hydrogen over platinum-based catalysts was proposed due to the suppression of OH groups formation on supports.

Unlike many WGS kinetic studies over different catalysts, current work did consider the presence of methane in the feed, and its subsequent effect on the reaction orders with respect to species involved for a CH_4 concentration of 7 %. The results revealed that any change in methane partial pressure had almost no effect on the forward reaction, which can also be verified by the apparent reaction orders of -0.0018 and 0.0015 evaluated for 1Pt-1Re-1Na/CeO_2 and 1Pt-1Re-1Na/TiO_2, respectively.

In order to evaluate the effect of partial pressures of the species involved in WGS (CO, H_2O, CO_2 and H_2) on the experimental reaction rates obtained for 1Pt-1Re-1Na/CeO_2 and 1Pt-1Re-1Na/TiO_2, the natural logarithm of [CO consumption rate / (1-β')] was plotted against the partial pressures of the species (Figure 4.10 and 4.11). As shown in graphs, all relationships are linear, confirming the fitness of proposed power law type model for the target reaction. A negative or positive slope of the straight line in the graphs characterizes the reaction order with respect to the related species. In this sense, increasing CO_2 and H_2

concentrations in the feed stream leads to a reduction in the reaction rate, defined by a negative slope, while the opposite is true for CO and H_2O.

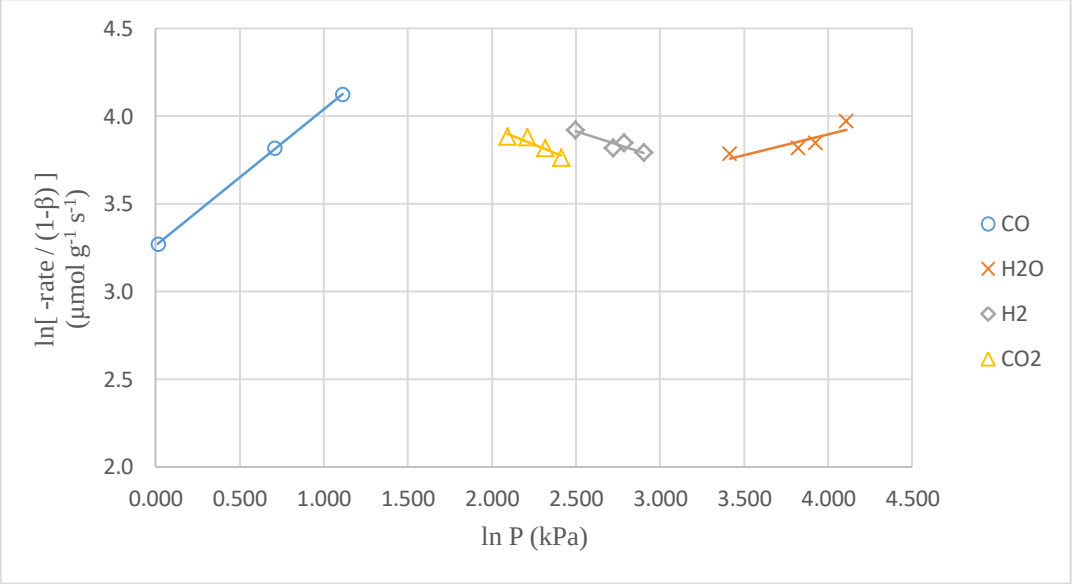

Figure 4.10. The effects of CO, H_2O, H_2, CO_2 partial pressures on WGS reaction rates for 1Pt-1Re-1Na/CeO_2

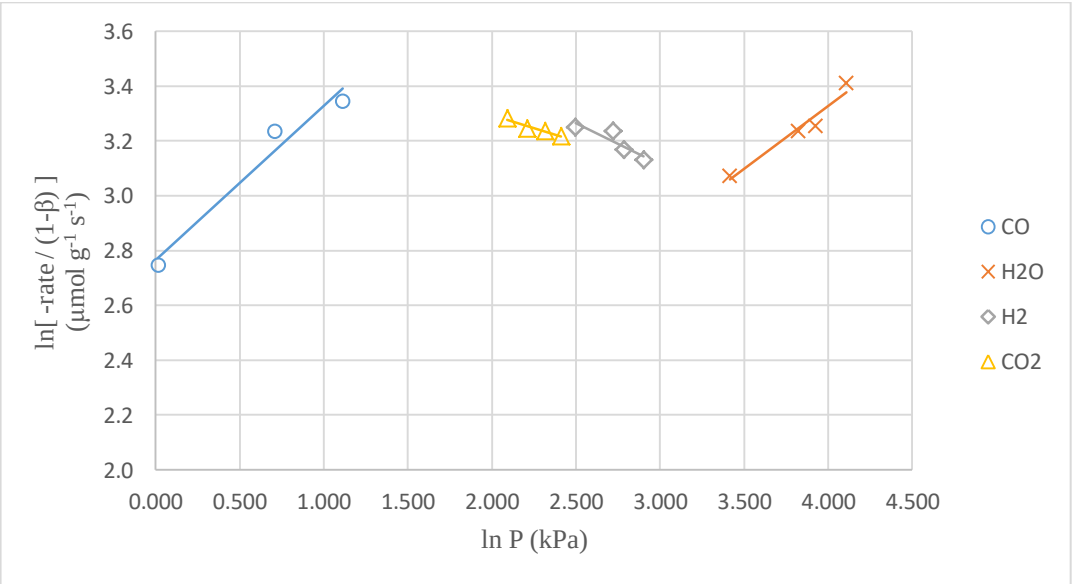

Figure 4.11. The effects of CO, H_2O, H_2, CO_2 partial pressures on WGS reaction rates for 1Pt-1Re-1Na/TiO_2

Based on the power values found for both catalysts, it can be concluded that the CeO_2 support is more sensitive to CO, which is more likely due to the high oxygen storage capacity (OSC) of ceria, while the opposite is true for TiO_2. In a study previously performed by our group (Öztürk, 2018), ceria supported Pt-based trimetallic catalysts demonstrated high OSC which is in accordance with the results obtained in current work.

According to the activity tests previously performed over the 1Pt-1Re-1Na/CeO_2 and 1Pt-1Re-1Na/TiO_2 catalysts, it was revealed that as the operating temperature was raised above 350 ^oC, the catalytic activity of the samples decreased (Eropak, B.M., 2020). Therefore, the base experiment (Run #2 in Table 3.6) was repeated at temperatures lower than 350 ^oC, at 300 and 325 °C, to calculate the apparent activation energy through using the Arrhenius equation (Equation 4.8). The activation energy (E_A) values and pre-exponential factor (k_0) estimated for both catalysts are summarized in Table 4.4, and the linearized form of Arrhenius equation (ln[rate/(1-β')] vs (1/T)) was plotted in Figure 4.8 in the temperature range of 300-350 °C. In the graph of ln[rate/(1-β')] against (1/T), the (E_A/R) term is equivalent to the slope of the straight line from which the activation energy was evaluated.

$$k = k_0 e^{(-\frac{E_A}{RT})} \tag{4.8}$$

Table 4.4. Kinetic parameters of WGS over 1Pt-0.5Re-1V/CeO_2 and 1Pt-0.5Re-1V/TiO_2

Catalyst Formula	**Parameter**	**Unit**	**Value**
1Pt-1Re-1Na/CeO_2	k_0	μmol $gcat^{-1}$ s^{-1} $kPa^{-0.49}$	948×10^3
	E_A	kJ mol^{-1}	51.072
1Pt-1Re-1Na/TiO_2	k_0	μmol $gcat^{-1}$ s^{-1} $kPa^{-0.49}$	446×10^3
	E_A	kJ mol^{-1}	69.533

An adequate comparison between the activation energies found in this study and those reported in the literature would be plausible in case of similar operating conditions such that the WGS feed is realistic, *and the inhibitory effect of H_2 and CO_2 is taken into account*. In this sense, the activation energies of 51.07 and 69.53 kJ mol^{-1} for 1Pt-1Re-

1Na/CeO_2 and 1Pt-1Re-1Na/TiO_2, respectively, found in the current study are in a good agreement with the results of Phatak *et al*. (2007), who reported the activation energy as 75 kJ/mol for the 1Pt/CeO_2 catalyst.

The effect of operating temperature and concentration of species involved in WGS reaction on the power-law type rate expressions for both the 1Pt-1Re-1Na/CeO_2 and 1Pt-1Re-1Na/TiO_2 catalysts are expressed in Equation 4.9 and 4.10, respectively.

$$-r_{CO} = [948 \times 10^3 e^{(-\frac{51072}{8.314 \times T})}] P_{CO}^{0.79} P_{H_2O}^{0.24} P_{H_2}^{-0.30} P_{CO_2}^{-0.31} P_{CH_4}^{-0.0018} (1 - \beta') \quad (4.9)$$

$$-r_{CO} = [446 \times 10^3 e^{(-\frac{69533}{8.314 \times T})}] P_{CO}^{0.57} P_{H_2O}^{0.45} P_{H_2}^{-0.30} P_{CO_2}^{-0.32} P_{CH_4}^{0.0015} (1 - \beta') \quad (4.10)$$

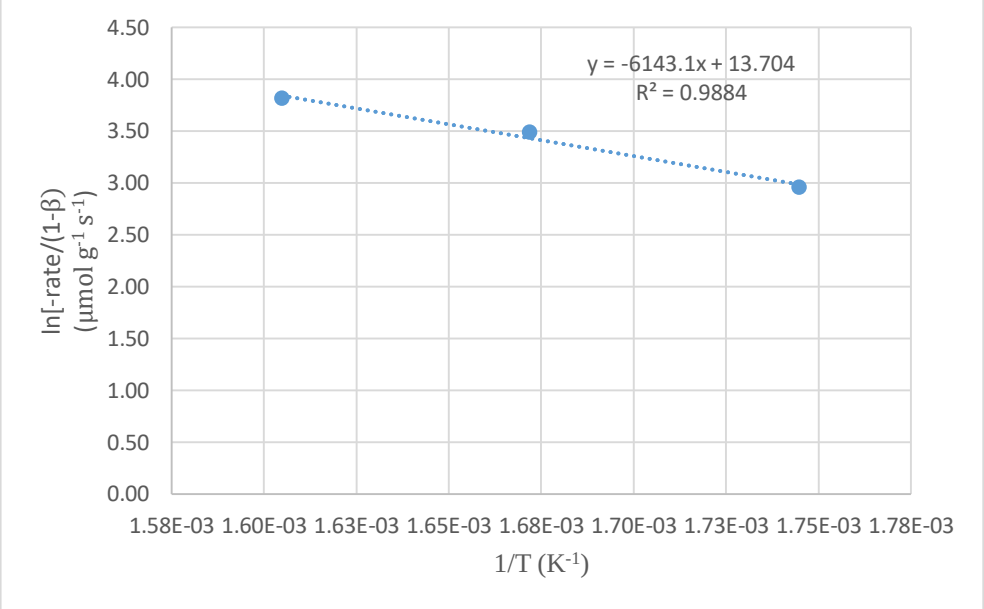

Figure 4.12. Arrhenius plot for WGS reaction over 1Pt-1Re-1Na/CeO_2

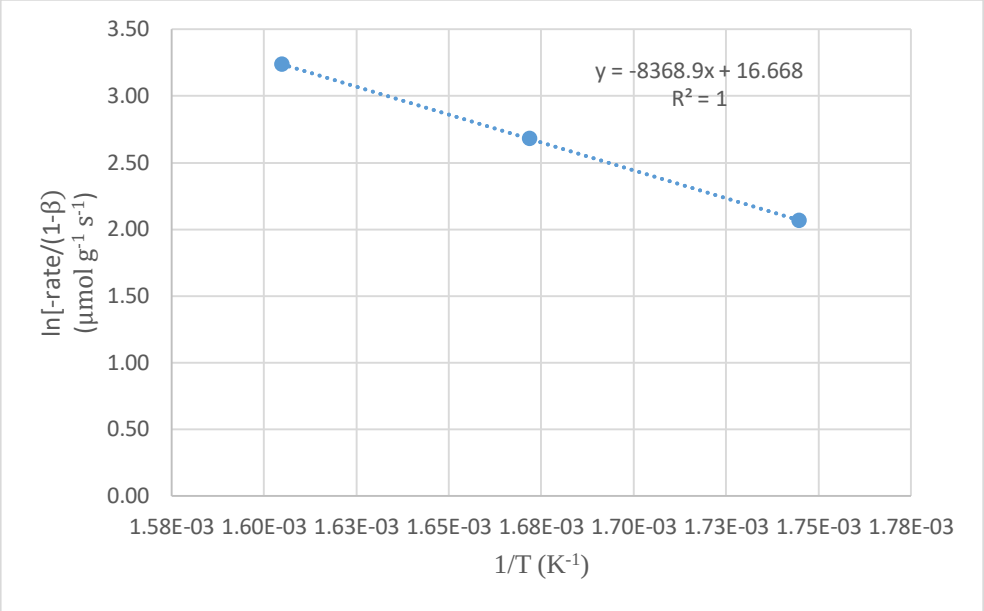

Figure 4.13. Arrhenius plot for WGS reaction over 1Pt-1Re-1Na/TiO_2

For both samples, the projected reaction rates (as given in Equation 4.9 and 4.10) were plotted against the experimentally obtained reaction rates in the intention to examine the accuracy of the proposed rate expressions. The corresponding plots in Figure 4.14 and 4.15 demonstrate that the developed power-law type rate expressions are reliable to predict the overall CO conversion rates quantitatively within 7 and 9% errors for the 1Pt-1Re-1Na/CeO_2 and 1Pt-1Re-1Na/TiO_2 samples, respectively.

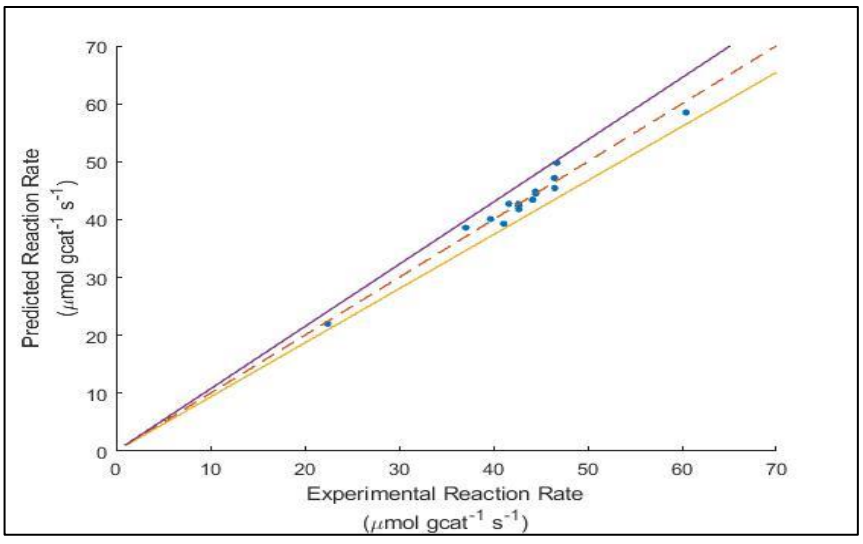

Figure 4.14. Experimental versus predicted reaction rates for 1Pt-1Re-1Na/CeO_2 within ± 7% error

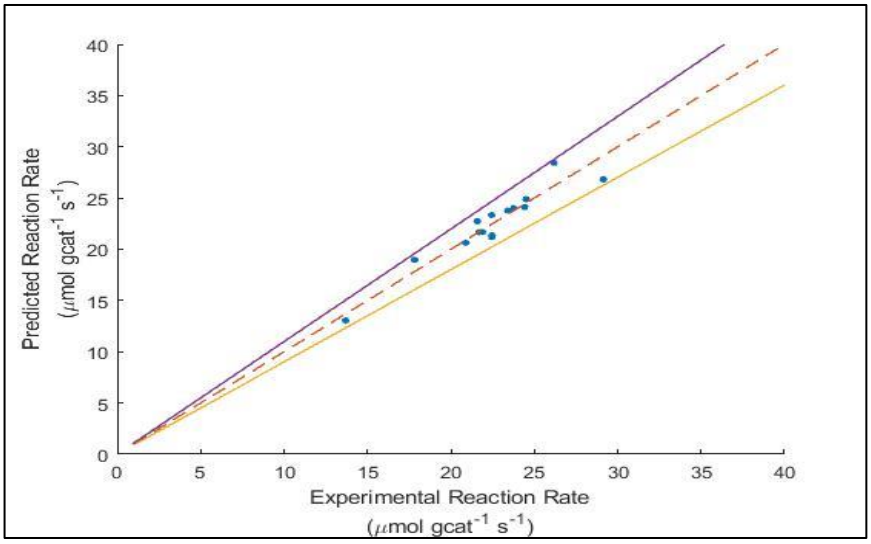

Figure 4.15. Experimental versus predicted reaction rates for 1Pt-1Re-1Na/TiO_2 within ± 9% error

5. CONCLUSIONS

5.1. Conclusions

As a successor of the former WGS performance studies carried out by our group (Eropak, 2020) over the 1Pt-1Re-1Na/CeO_2 and 1Pt-1Re-1Na/TiO_2 samples, the present study developed power-law type kinetic expressions for the target reaction over the same catalysts, which can be practical in the design of a WGS reactor for small-scale stationary fuel processor – fuel cell (FP-FC) applications. The kinetic tests were conducted under realistic conditions mimicking the product composition of the OSR reactor as the feed (Table 3.6) of the WGS reactor operating at 350 °C. Moreover, the effect of CH_4 concentration in the feed stream on WGS kinetics was also examined to determine the relationship between the methane partial pressure and rate of WGS reaction.

For each of the catalysts, 15 pairs of kinetic experiments *(total of 30)* were performed by changing the concentrations of the species involved in reaction and contact/residence time. The power-law kinetic model of WGS reaction over 1Pt-1Re-1Na/CeO_2 and 1Pt-1Re-1Na/TiO_2 catalysts was estimated by using the method of initial rates within ±7% and ±9% error, respectively. The reaction orders for the proposed kinetic model over 1Pt-1Re-1Na/CeO_2 catalyst were obtained as 0.79, 0.24, -0.30, -0.31 and -0.0018 for CO, H_2O, H_2, CO_2 and CH_4, respectively, while those over the 1Pt-1Re-1Na/TiO_2 sample were estimated as 0.57, 0.45, -0.30, -0.31 and 0.0015 for the same reactants sequence by non-linear regression analysis performed in MATLAB^{TM}.

The rate expressions were obtained with positive dependence on CO and H_2O. Negative reaction orders with respect to CO_2 and H_2O were obtained, which indicated the inhibitory effect of CO_2 and H_2O on the reaction rate. Since the reaction order with respect to CH_4 was of -0.0018 and 0.0015 for 1Pt-1Re-1Na/CeO_2 and 1Pt-1Re-1Na/TiO_2, it can be concluded that there was no methane effect on the reaction rate. The apparent activation energies of 51.07 and 69.53 kJ mol^{-1} and frequency factors of 948 μmol $mgcat^{-1}$ s^{-1} $kPa^{-0.42}$ and 446 μmol $mgcat^{-1}$ s^{-1} $kPa^{-0.40}$ were obtained for 1Pt-1Re-1Na/CeO_2 and 1Pt-1Re-1Na/TiO_2, respectively in a temperature range of 300-350 ºC.

5.2. Recommendations

The following further works can be performed considering the results obtained in the current study as a basis:

- To achieve more accurate results, the kinetic experiments can be repeated for three or more residence time values;

- An *operando* FTIR-DRIFTS-MS analysis can be conducted over the same samples to examine reaction mechanisms and effect of support type;

- The power-law type rate models can also be derived for Pt-Na/CeO_2 or Pt-Re/CeO_2 and Pt-Na/TiO_2 or Pt-Re/TiO_2 to understand the role of promoters in Pt-Re-Na/CeO_2 and Pt-Re-Na/TiO_2.

- Mechanistic Langmuir Hinshelwood Hougen-Watson (LHHW) type models can be developed for both catalysts under similar operating conditions.

6. REFERENCES

Ahmed, A., Q. A. Al-Amin, F. A. Ambrose and R. Saidur, "Hydrogen Fuel and Transport System: A Sustainable and Environmental Future", *International Journal of Hydrogen Energy*, Vol. 41, pp.1369-1380, 2016.

Andrea, M., D. Farias, P. Bargiela, M. C. Rocha and M. A. Fraga, "Vanadium Promoted Pt/CeO_2 Catalyst for Water-Gas Shift Reaction", *Journal of Catalysis*, Vol. 260, pp. 93-102, 2008.

Azzam, K. G., I. V. Babich, K. Seshan and L. Lefferts, "Role of Re in $Pt\text{-}Re/TiO_2$ Catalyt for Water-Gas Shift Reaction: A Mechanistic and Kinetic Study", *Applied Catalysis B: Environmental*, Vol. 80, pp. 129-140, 2006.

Başar, M., *A Study on CO-free Hydrogen Production and Adsorbent Design for Selective Carbon Dioxide Removal*, Doctor of Philosophy Thesis, Boğaziçi University, 2016.

Başar, M. S., B. S. Çağlayan and A. E. Aksoylu, "A Study on Catalytic Hydrogen Production: Thermodynamic and Experiemental Analysis of Serial OSR-PROX System", *Fuel Processing Technology*, Vol. 178, pp. 301-311, 2018.

Çağlayan, B. S. and A. E Aksoylu, "Water-Gas Shift Reaction over Bimetallic $Pt\text{-}Ni/Al_2O_3$ Catalysts", *Turkish Journal of Chemistry*, Vol. 33, pp. 249-256, 2009.

Çağlayan, B. S. and A. E. Aksoylu, "Water–Gas Shift Activity of Ceria Supported Au–Re Catalysts", *Catalysis Communications*, Vol. 12, pp. 1206-1211, 2011.

Castano, M. G., T. R. Reina, S. Ivanova, M. A. Centeno and J. A. Odriozola, "Pt vs Au in Water-Gas Shift Reaction", *Journal of Catalysis*, Vol. 314, pp. 1-9, 2014.

Cipriani, G., V. D. Dio, F. Genduso, D. La Cascia, R. Liga, R. Miceli and G. R. Galluzzo, "Perspective on Hydrogen Energy Carrier and Its Automotive Applications", *International Journal of Hydrogen Energy*, Vol. 39, pp. 8482-8494, 2014.

Cui, Z. and S. K. Kaer, "Thermodynamic Analysis of Steam Reforming and Oxidative Steam Reforming of Propane and Butane for Hydrogen Production", *International Journal of hydrogen Energy*, Vol. 43, pp. 13009-13021, 2018.

Demirhan, C., *Design and Development of WGS Catalysts for Small-scale Hydrogen Production Units*, Master of Science Thesis, Boğaziçi University, 2015.

Ercolino, G., M. A. Ashraf, V. Specchia and S. Specchia, "Performance Evaluation and Comparison of Fuel Processors Integrated with PEM Fuel Cell based on Steam or Autothermal Reforming and on CO Preferential Oxidation or Selective Methanation", *Applied Energy*, Vol. 143, pp. 138-153, 2015.

Eropak, B. M. and A. E. Aksoylu, "A Reliable Power-Law Type Kinetic Expression for PROX over Pt-Sn/AC", *Catalysis Communication*, Vol. 95, pp.67-71, 2017.

Eropak, B. M., *A Study on CO-Free Hydrogen Production from Hydrocarbons and CO_x Elimination Through Pre-Combustion*, Doctor of Philosophy (PhD) Thesis, Boğaziçi University, 2020.

Gamboa-Rosales, N. K., J. L. Ayastuy and M. A. Gutierrez-Ortiz, "Effect of Au in Au-Co_3O_4/CeO_2 Catalyt During Oxygen-Enhanced Water-Gas Shift", *International Journal of Hydrogen Energy* , Vol. 41, pp. 19408-19417, 2016.

Gökaliler, F., B. S. Çağlayan, Z. İ. Önsan and A. E. Aksoylu, "Hydrogen Production by Autothermal Reforming of LPG for PEM Fuel Cell Applications", *International Journal of Hydrogen Energy*, Vol. 33, pp. 1383-1391, 2008.

Gonzalez, I. D., R. M. Navarro, W. Wen, N. Marinkovic, J. A. Rodriguez, F. Rosaand J. L. G. Fierro, "A Comparative Study of the Water-Gas Shift Reaction over Platinum Catalysts Supported on CeO_2, TiO_2 and Ce-modified TiO_2", *Catalysis Today*, Vol. 149, pp. 372-379, 2010.

Gradisher, L., B. Dutcher and M. Fan, "Catalytic Hydrogen Production from Fossil Fuels via the Water-Gas Shift Reaction", *Applied Energy*, Vol. 139, pp. 335-349, 2015.

Guo, P. J., L. F. Chen, Y. Guo-Bin, Y. Zhu, M. H. Qiao, H. L. Xu and K. N. Fan, "Cu/ZnO-based Water–Gas Shift Catalysts in Shut-down/Start-up Operation", *Catalysis Communications*, Vol. 10, pp. 1252-1256, 2011.

Hakeem, A. A., M. Li, R. J. Berger, F. Kaptejin and M. Makkee, "Kinetics of the High Temperature Water–Gas Shift over Fe_2O_3/ZrO_2, Rh/ZrO_2 and $Rh/Fe_2O_3/ZrO_2$", *Chemical Engineering Journal*, Vol. 263, pp. 427-434, 2015.

Hla, S. S., D. Park, G. J. Duffy, J. H. Edwards, D. G. Roberts, A. Ilyushechkin, L. D. Morpeth and T. Nguyen, "Kinetics of High-Temperature Water-Gas Shift Reaction over Two Iron-based Commercial Catalysts using Simulated Coal-derived Syngases", *Chemical Engineering Journal*, Vol. 146, pp. 148-154, 2009.

Hla, S. S., Y. Sun, G. J. Duffy, L. D. Morpeth, A. Ilyushechkin, A. Cousins, D. Roberts and J. H. Edwards, "Kinetics of the Water-Gas Shift Reaction over a $La_{0.7}Ce_{0.2}FeO_3$ Perovskite-like Catalyst using Simulated Coal-derived Syngas at a High Temperature", *International Journal of Hydrogen Energy*, Vol. 36, pp. 518-527, 2011.

Holladay, J. D., J. Hu, D. King and Y. Wang, "An Overview of Hydrogen Production Technologies", *Catalysis Today*, Vol. 139, pp. 244-260, 2009.

Jeong, D. W., W. Jang, J. O. Shim, W. B. Han, H. S. Roh, U. H. Jun and W. L. Yoon, "Low-Temperature Water-Gas Shift Reaction over Supported Cu Catalysts", *Renewable Energy*, Vol. 65, pp. 102-107, 2013.

Jeong, D. W., H. S. Potdar, J. O. Shim, W. J. Jang and H. S. Roh, "H_2 Production from a Single Stage Water-Gas Shift Reaction over Pt/CeO_2, Pt/ZrO_2, and $Pt/Ce_{(1-x)}Zr_{(x)}O_2$ Catalysts", *International Journal of Hydrogen Energy*, Vol. 38, pp. 402-407, 2013.

Kalamaras, C. M., P. Panagiotopoulou, D. I. Kondarides and A. Efsathiou, "Kinetic and Mechanistic Studies of Water-Gas Shift Reaction on Pt/TiO_2 Catalyst", *Journal of Catalysis* , Vol. 264, pp. 117-129, 2009.

Karakaya, C., R. Otterstatter, L. Maier and O. Deutschmann, "Kinetics of Water-Gas Shift Reaction over Rh/Al_2O_3 Catalysts", *Applied Catalysis A: General*, Vol. 470, pp. 31-44, 2014.

Koroneos, C., A. Dompros, G. Roumbas and N. Moussiopoulos, "Life Cycle Assessment of Hydrogen Fuel Production Processes, *International Journal of Hydrogen Energy*, Vol. 29, pp. 1443-1450, 2004.

Koryabkina, N. A., A. A. Phatak, W. F. Ruettinger and H. Ribeiro, "Determination of Kinetic Parameters for the Water-Gas Shift Reaction on Copper Catalysts under Realistic Conditions for Fuel Cell Applications", *Journal of Catalysis*, Vol. 217, pp. 233-239, 2003.

Leppelt, R., B. Schumacher, V. Plzak, M. Kinne and R. J. Behm, "Kinetics and Mechanism of the Low Temperature Water–Gas Shift Reaction on Au/CeO_2 Catalysts in an Idealized Reaction Atmosphere", *Journal of Catalysis*, Vol. 244, pp. 137-152, 2006.

Lototskyy, M. V., I. Tolj, L. Pickering, C. Sita, F. Barbir and V. Yartys, "The Use of Metal Hydrides in Fuel Cell Applications", *The Progress in Natural Sciences: Materials International*, Vol. 27, pp. 3-20, 2017.

Meunier, F. C., G. Yablonsky, D. Reid, S. O. Shekhtman, C. Hardacre, R. Burch and M. Lazman, "Negative Apparent Kinetic Order in Steady-state Kinetics of the Water-Gas Shift Reaction over a Pt/CeO_2 Catalyst", *Catalysis Today*, Vol. 138, pp. 216-221, 2008.

Mohamed, Z., V. Dasireddy, S. Singh and H. B. Friedrich, "The Preferential Oxidation of CO in Hydrogen Rich Streams over Platinum Doped Nickel Oxide Catalysts", *Applied Catalysis B: Environmental*, Vol. 180, pp. 689-697, 2007.

Moreno, M., G. T. Baronetti, M. A. Laborde and F. J. Marino, "Kinetics of Preferential CO Oxidation in H_2 Excess (COPROX) over CuO/CeO_2 Catalysts", *International Journal of Hydrogen Energy*, Vol. 33, pp. 3538-3542, 2008.

Na, H. S., J. O. Shim, W. Jang, K. W. Jeon H. M. Kim, Y. L. Lee, D. Lee, S. Y. Yoo and H. S. Roh, "The Effect of Titration Time on the Catalytic Performance of Cu/CeO_2 Catalysts for Water-Gas Shift Reaction", *Catalysis Today*, Vol. 309, pp. 83-88, 2019.

Opalka, S. M., T. H. Vanderspurt, R. Radhakrishnan, Y. She and R. R. Wiligan, "Design of Water-Gas Shift Catalysts for Hydrogen Production in Fuel Processors", *Journal of Physics: Condensed Matter*, Vol. 20, pp. 1-12, 2008.

Öztürk, G., *An Experimental Study on WGS Catalysts: Relating Performance under Real Feed with Oxygen Holding Capacity*, Master of Science Thesis, Boğaziçi University, 2008.

Özyönüm, G. N. and R. Yildirim, "Water-Gas Shift Activity of Au-Re Catalyst over Microstructured Cordierite Monolith Wash-coated by Ceria", *International Journal of Hydrogen Energy*, Vol. 41, pp. 5513-5521, 2016.

Pal, D. B., R. Chand, S. Updahyay and P. K. Mishra, "Performance of Water-Gas Shift Reaction: A Review", *Renewable and Sustainable Energy Reviews*, Vol. 93, pp. 549-565, 2018.

Pasel, J., R. C. Samsun, A. Tschauder, R. Peters and D. Stolten, "Water-Gas Shift Reactor for Fuel Cell Systems: Stable Operation for 5000 Hours", *International Journal of Hydrogen Energy*, Vol. 43, pp. 19222-19230., 2018.

Pastor-Perez, L., V. Belda-Alcazar, C. Marini, M. M. Pastor-Blas, A. Sepulveda-Escribano and W. V. Ramos-Fernandez, "Effect of Cold Ar Plasma Treatment on the Catalytic Performance of Pt/CeO_2 in Water-Gas Shift Reaction", *Applied Catalysis B: Environmental*, Vol. 225, pp. 121-127, 2018.

Perez, P., M. A. Soria, A. C. Carabineiro, F. J. Maldonado-Hodar, A. Mendes and L. M. Madeira, "Application of Au/TiO_2 Catalysts in the Low-Temperature Water-Gas Shift Reaction", *International Journal of Hydrogen Energy*, Vol. 41, pp. 4670-4681, 2016.

Phatak, A. A., N. Koryabkina, S. Rai, J. L. Ratts, W. Ruettinger, R. J. Farrauto, G. R. Blau, Delgass and F. H. Ribeiro, "Kinetics of the Water–Gas Shift Reaction on Pt Catalysts Supported on Alumina and Ceria", *Catalysis Today*, Vol. 123, pp. 224-234, 2007.

Plaza, A., S. Fail, J. A. Cortes, J. Fottinger, N. Diaz, R. Rauch and H. Hofbauer, "Apparent Kinetics of the Catalyzed Water-Gas Shift Reaction in Synthetic Wood Gas", *Chemical Engineering Journal*, Vol. 301, pp. 222-228, 2006.

Radhakrishnan, R., R. R. Willigan, Z. Dardas and T. H. Vanderspurt, "Water-Gas Shift Activity and Kinetics of Pt/Re Catalysts Supported on Ceria-Zirconia Oxides", *Applied Catalysis B: Environmental*, Vol. 66, pp. 23-28, 2006.

Rodriguez, J., "Gold-based Catalysts for the Water–Gas Shift Reaction: Active Sites and Reaction Mechanism", *Catalysis Today*, Vol. 160, pp. 3-10, 2011.

Rodriguez, J. A., P. J. Ramírez and R.A. Gutierrez, "Highly Active Pt/MoC and Pt/TiC Catalysts for the Low-Temperature WGS Reaction: Effects of the Carbide Metal/Carbon Ratio on the Catalyst Performance", *Catalysis Today*, Vol. 289, pp. 47-52, 2017.

Runxia, H., W. Dandan, Z. Keuduan, Z. Huacong, J. Haoqianq, L. Na and L. Quansheng, "Cu-Mn Catalysts Modified by Rare Earth Lantnaum for Low Temperature Water-Gas Shift Reaction", *Journal of Rare Earths*, Vol. 34, pp. 994-1003, 2016.

Saeidi, S., F. Fazlollahi, S. Najari, D. Iranshahi, J. J. Klemes and L. Baxter, "Hydrogen Production: Perspectives, Separation with Special Emphasis on Kinetics of WGS Reaction: A State-of-the-Art Review", *Journal of Industrial and Engineering Chemistry*, Vol. 49, pp. 1-25, 2016.

Sato, Y., K. Terada, Y. Soma, T. Miyao and A. Natio, "Marked Addition Effect of Re upon the Water-Gas Shift Reaction over TiO_2 Supported Pt, Pd and Ir Catalysts", *Catalysis Communications*, Vol. 7, pp. 91-95, 2005.

Sengodan, S., R. Lan, J. Humphreys, D. Du, H. Wan and S. Tao, "Advances in Reforming and Partial Oxidation of Hydrocarbons for Hydrogen Production and Fuel Cell Applications", *Renewable and Sustainable Energy Reviews*, Vol. 82, pp. 761-780, 2018.

Sigh, S., S. Jain, P. S. Venkateswaran, K. A. Twiwari, R. M. Nouni, K. J. Pandey and S. Goel, "Hydrogen: A Sustainable Fuel for Future of the Transport Sector", *Renewable and Sustainable Energy Reviews*, Vol. 51, pp. 623-633, 2015.

Thinon O., K. Rachedi, F. Diehl, P. Avenie and Y. Schurman, "Kinetics and Mechanism of the Water–Gas Shift Reaction over Platinum Supported Catalysts", *Topics in Catalysis*, Vol. 52, pp. 1940-1945, 2009.

Thouchprasitchai, N., A. Luengnaruemitchai and S. Pongstabodee, "The Activities of Cu-based Mg-Al Layered Double Oxide Catalysts in the Water-Gas Shift Reaction", *International Journal of Hydrogen Energy* , Vol. 41, pp. 14147-14159, 2006.

Trimm, D. L. and Z. İ. Önsan, "Onboard Fuel Conversion for Hydrogen-Fuel-Cell-Driven-Vehicles", *Catalysis Reviews*, Vol. 43, pp. 31-84, 2011.

Venkata, D. B. C. D., B. Likoza and J. Valand, "Preferential Oxidation of CO in $H_2/H_2O/CO_2$ Water–Gas Shift Feedstocks over Cubased Carbon Nanotube supported Heterogeneous Catalysts, *Applied Catalysis B: Environmental*", Vol. 237, pp. 1044-1058, 2008.

Vindigni, F., M. Manzoli, T. Tabakova, V. Idakiev, F. Bocuzzi and A. Chiorino, "Gold Catalysts for Low Temperature Water-Gas Shift Reaction: Effect of ZrO_2 Addition to CeO_2 Support", *Applied Catalysis B: Environmental*, Vol. 125, pp. 507-515, 2012.

Wang, G., Y. Yu, H. Liu, C. Gong, S. Wen, X. Wang and Z. Tu, "Progress on Design and Development of Polymer Electrolyte Membrane Fuel Cell Systems for Vehicle Applications: A Review", *Fuel Processing Technology*, Vol. 179, pp. 203-228, 2011.

Xu, X., Q. Fu and X. Bao, "MoOx-Promoted Pt Catalysts for the Water-Gas Shift Reaction at Low Temperatures", *Chinese Journal of Catalysis*, Vol. 36, pp. 750-756, 2015.

Yan, H., X. T. Qin, Y. Yin, Y. Teng, Z. Jin and C. J. Jia, "Promoted Cu-Fe_3O_4 Catalysts for Low-Temperature Water-Gas Shift Reaction: Optimization of Cu Content", *Applied Catalysis B: Environmental*, Vol. 226, pp. 182-193, 2018.

Yu, Q., W. Chen, Y. Li, M. Jin and Z. Suo, "The action of Pt in bimetallic Au–Pt/CeO_2 catalyst for water–gas shift reaction", *Catalysis Today*, Vol. 158, pp. 324-328, 2010.

Yumru, G., *WGS Kinetics over Pt-based Trimetallic Catalyst Sytems under Realistic Condistions*, Master of Science Thesis, Boğaziçi University, 2017.

Zhu, X., M. Shen, L .L. Lobban and R.G. Mallinson, "Structural Effects of Na Promotion for High Water-Gas Shift Activity on Pt–Na/TiO_2", *Journal of Catalysis*, Vol. 278, pp. 123-132, 2011.

7. APPENDIX A: CONVERSION VERSUS RESIDENCE TIME GRAPHS FOR 1Pt-1Re-1Na/TiO_2 and 1Pt-1Re-1Na/TiO_2

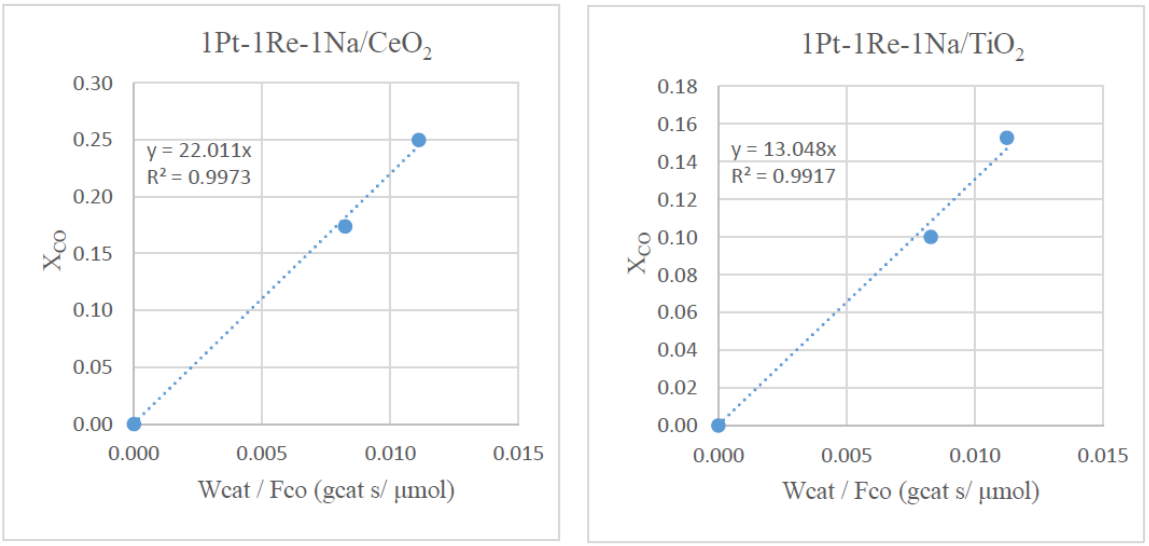

Figure A.1. A graph of CO conversion against residence time for Run #1 conducted at 350 ^oC over 1Pt-1Re-Na/CeO_2 (to the left) and 1Pt-1Re-1Na/TiO_2 (to the right)

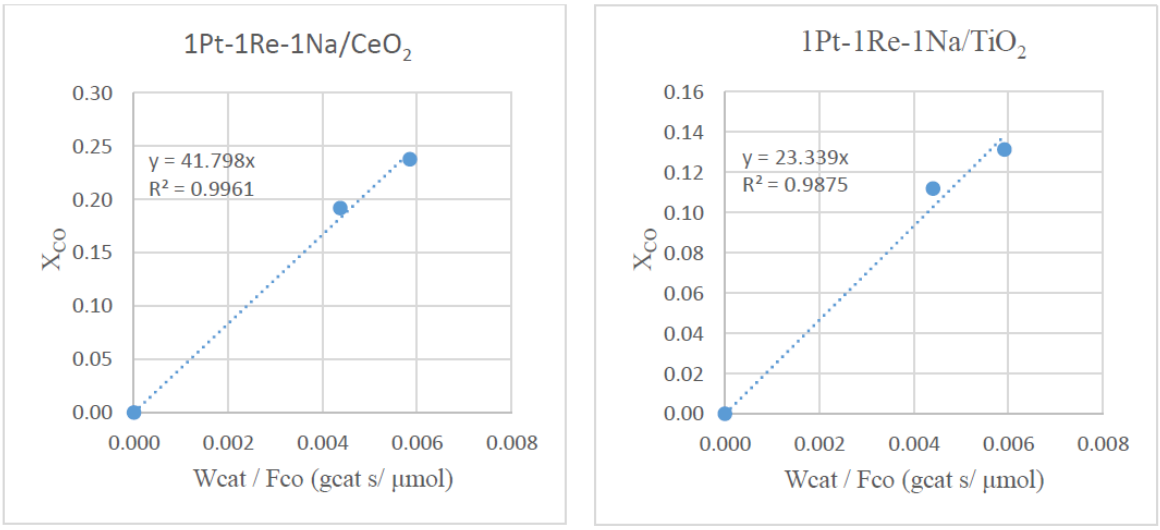

Figure A.2. A graph of CO conversion against residence time for Run #2 conducted at 350 ^oC over 1Pt-1Re-Na/CeO_2 (to the left) and 1Pt-1Re-1Na/TiO_2 (to the right)

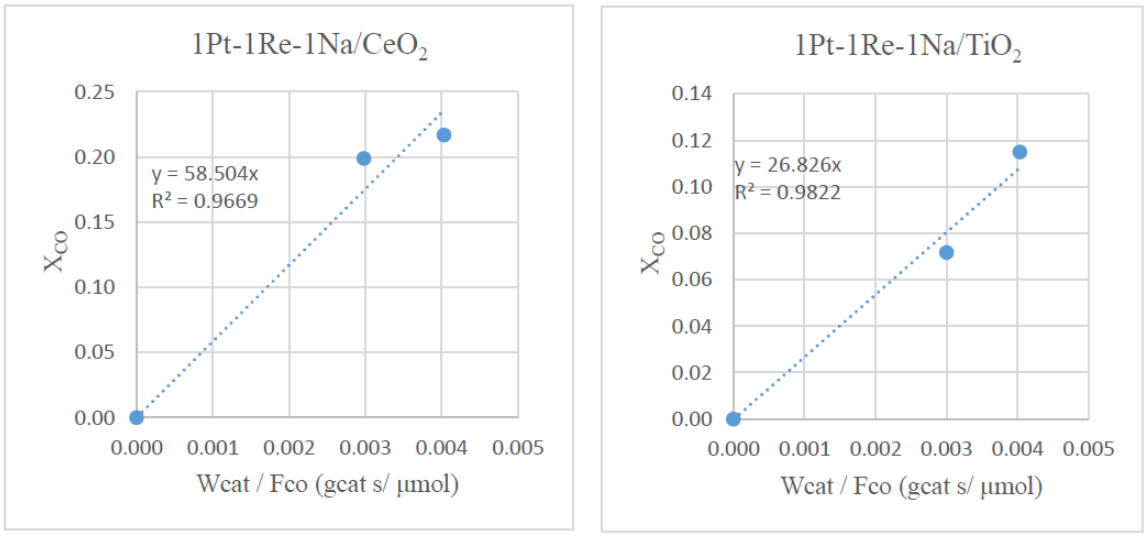

Figure A.3. A graph of CO conversion against residence time for Run #3 conducted at 350 ^{o}C over 1Pt-1Re-Na/CeO_2 (to the left) and 1Pt-1Re-1Na/TiO_2 (to the right)

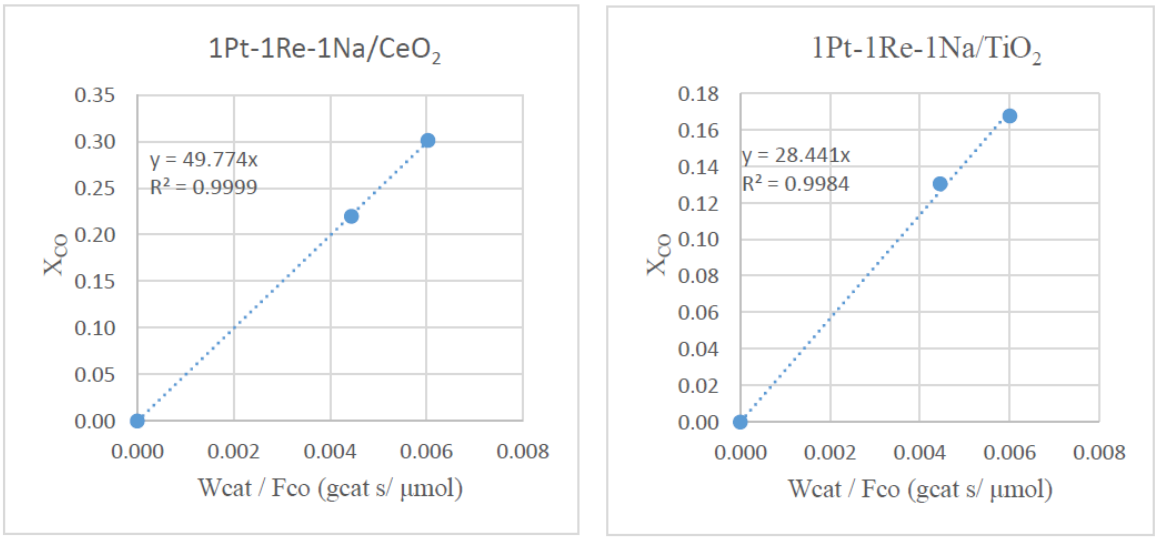

Figure A.4. A graph of CO conversion against residence time for Run #4 conducted at 350 ^{o}C over 1Pt-1Re-Na/CeO_2 (to the left) and 1Pt-1Re-1Na/TiO_2 (to the right)

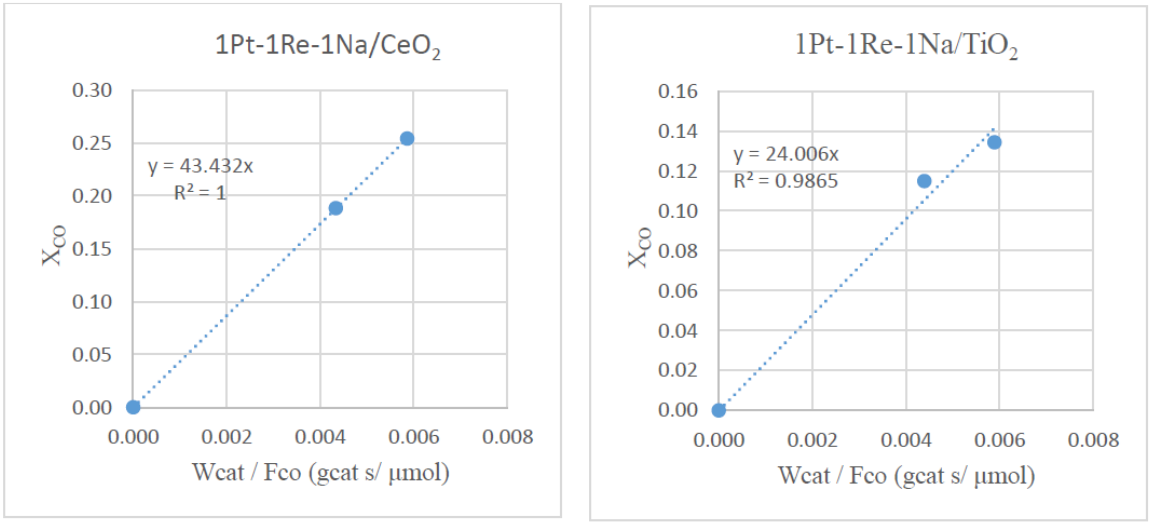

Figure A.5. A graph of CO conversion against residence time for Run #5 conducted at 350 ^{o}C over 1Pt-1Re-Na/CeO_2 (to the left) and 1Pt-1Re-1Na/TiO2 (to the right)

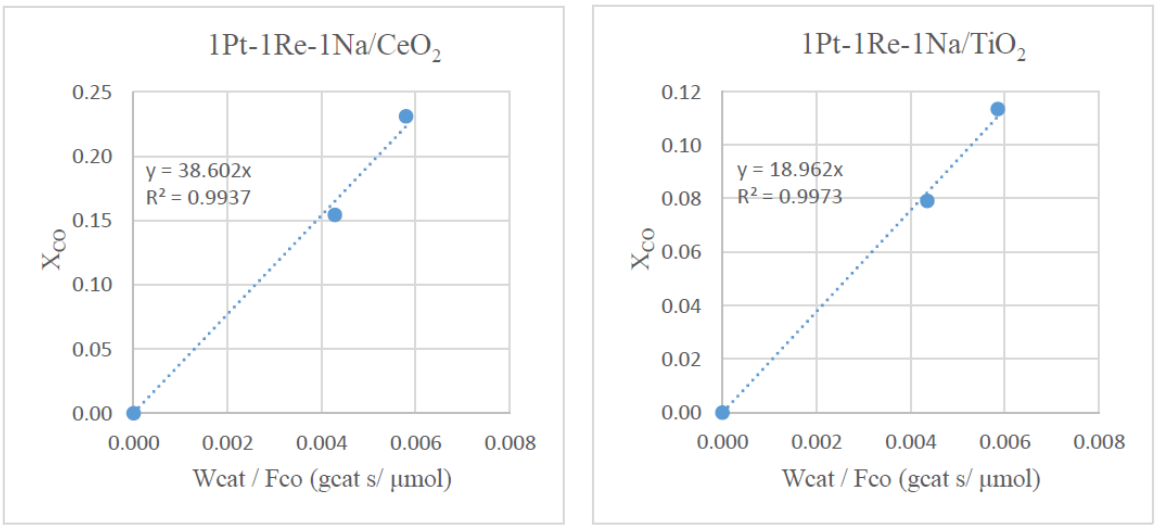

Figure A.6. A graph of CO conversion against residence time for Run #6 conducted at 350 ^{o}C over 1Pt-1Re-Na/CeO_2 (to the left) and 1Pt-1Re-1Na/TiO_2 (to the right)

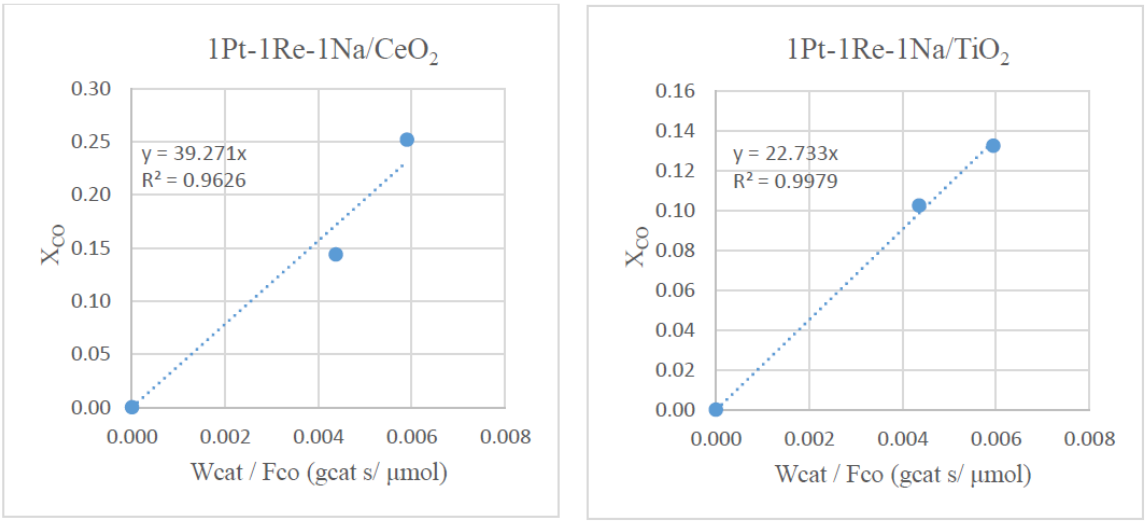

Figure A.7. A graph of CO conversion against residence time for Run #7 conducted at 350 ^{o}C over 1Pt-1Re-Na/CeO_2 (to the left) and 1Pt-1Re-1Na/TiO_2 (to the right)

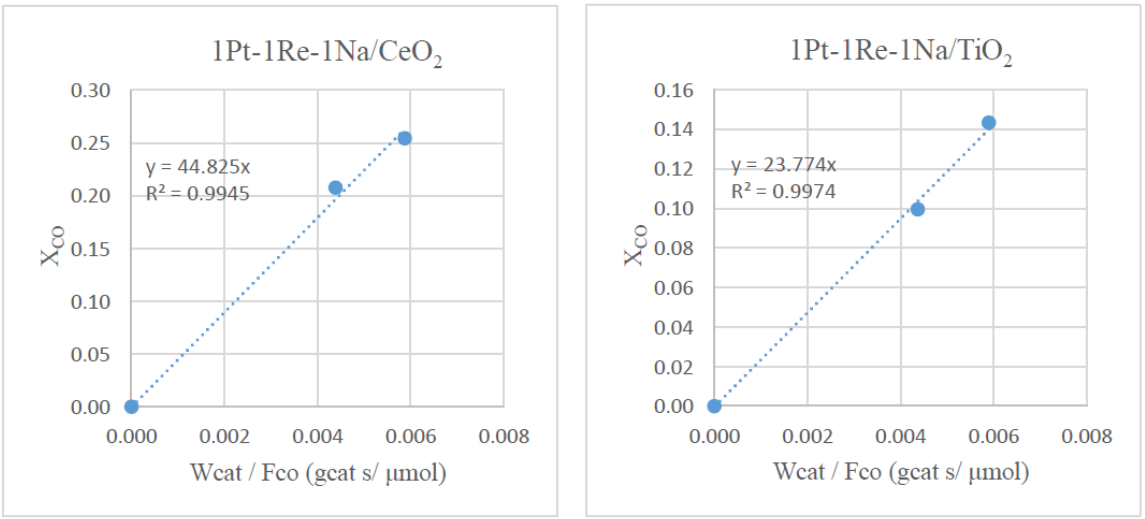

Figure A.8. A graph of CO conversion against residence time for Run #8 conducted at 350 ^{o}C over 1Pt-1Re-Na/CeO_2 (to the left) and 1Pt-1Re-1Na/TiO_2 (to the right)

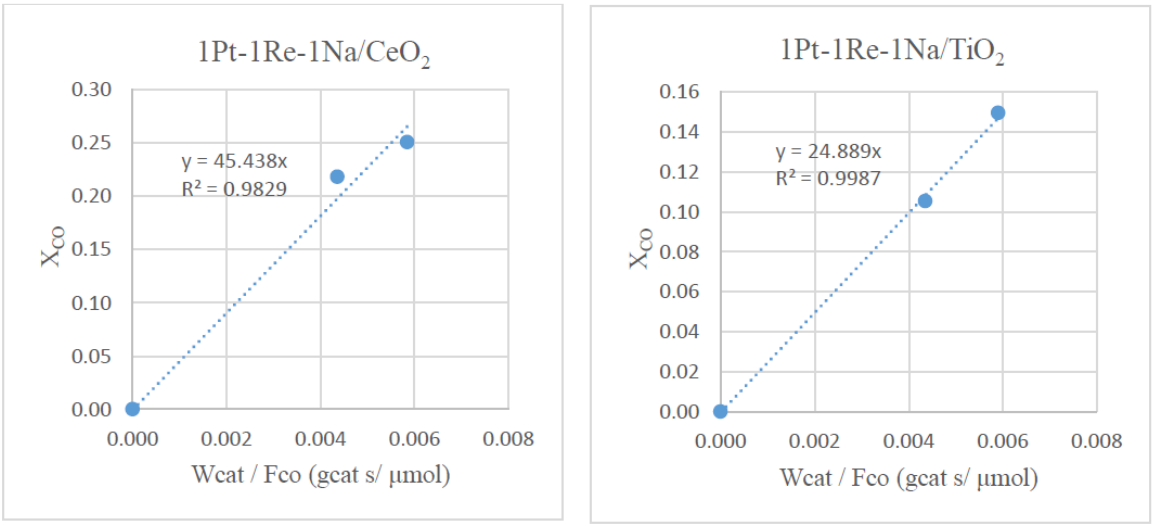

Figure A.9. A graph of CO conversion against residence time for Run #9 conducted at 350 ^{o}C over 1Pt-1Re-Na/CeO_2 (to the left) and 1Pt-1Re-1Na/TiO_2 (to the right)

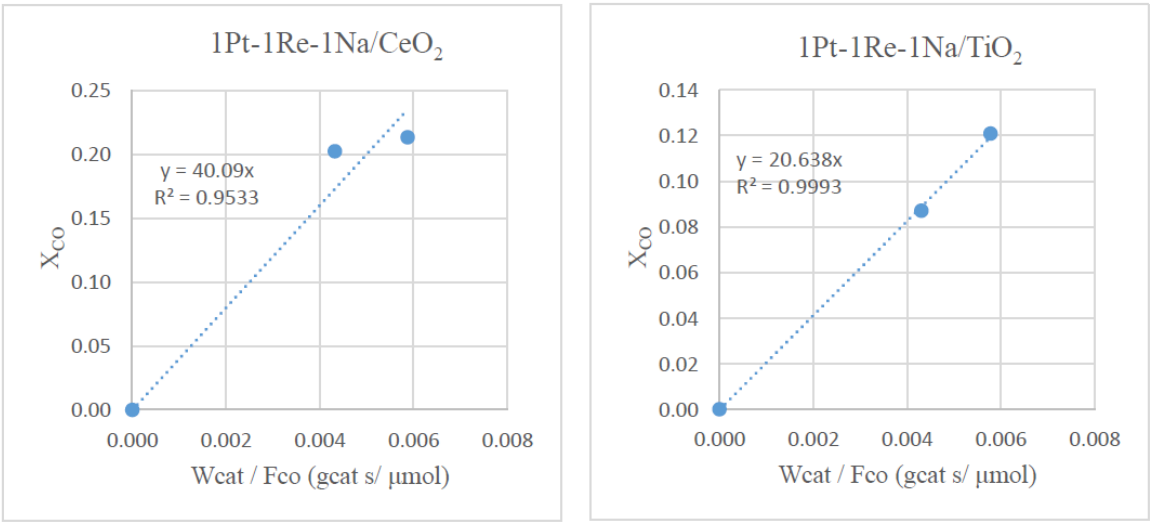

Figure A.10. A graph of CO conversion against residence time for Run #10 conducted at 350 ^{o}C over 1Pt-1Re-Na/CeO_2 (to the left) and 1Pt-1Re-1Na/TiO_2 (to the right)

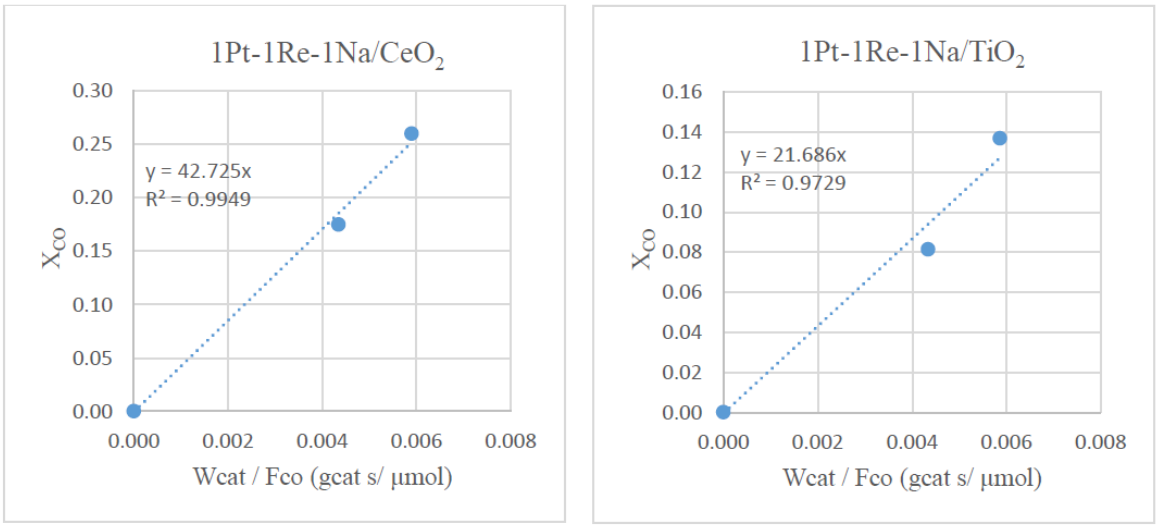

Figure A.11. A graph of CO conversion against residence time for Run #11 conducted at 350 ^{o}C over 1Pt-1Re-Na/CeO_2 (to the left) and 1Pt-1Re-1Na/TiO_2 (to the right)

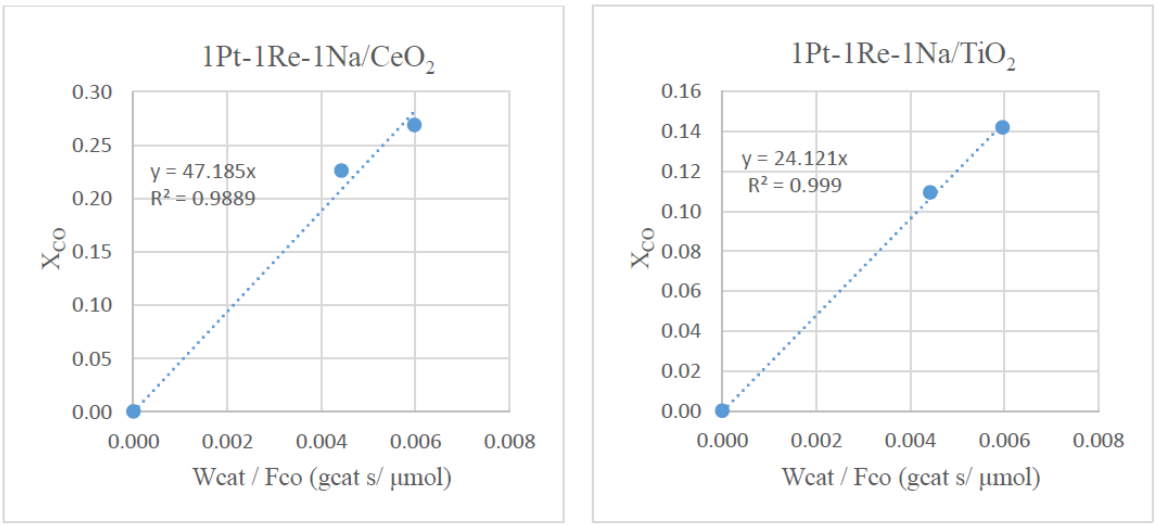

Figure A.12. A graph of CO conversion against residence time for Run #12 conducted at 350 ^{o}C over 1Pt-1Re-Na/CeO_2 (to the left) and 1Pt-1Re-1Na/TiO_2 (to the right)

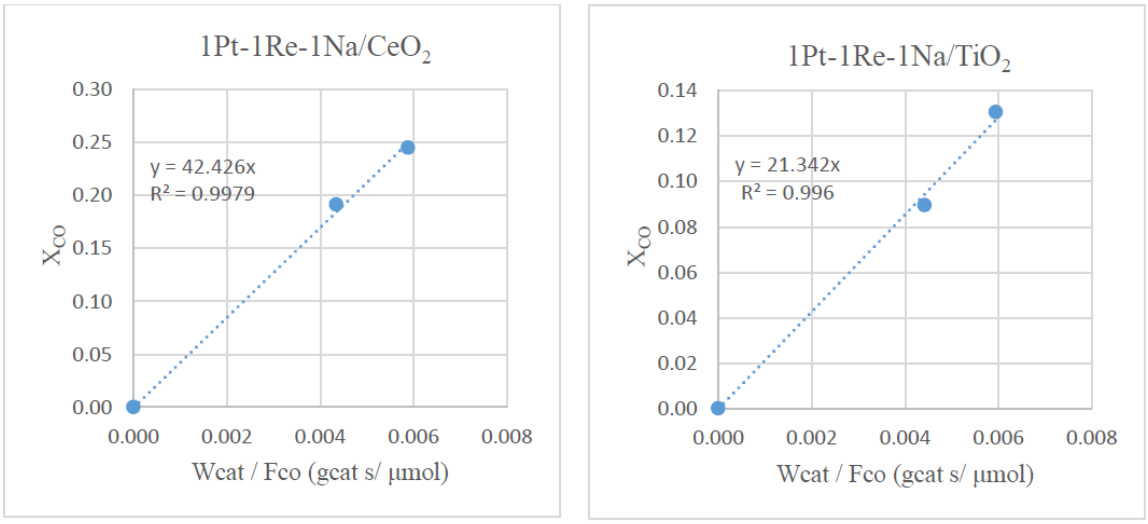

Figure A.13. A graph of CO conversion against residence time for Run #13 conducted at 350 ^{o}C over 1Pt-1Re-Na/CeO_2 (to the left) and 1Pt-1Re-1Na/TiO_2 (to the right)

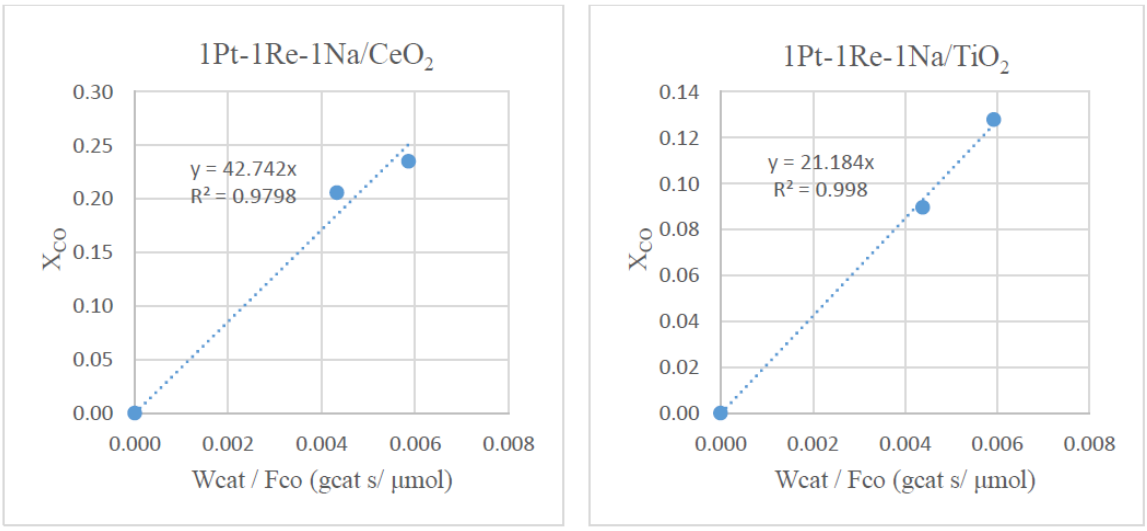

Figure A.14. A graph of CO conversion against residence time for Run #14 conducted at 350 ^{o}C over 1Pt-1Re-Na/CeO_2 (to the left) and 1Pt-1Re-1Na/TiO_2 (to the right)

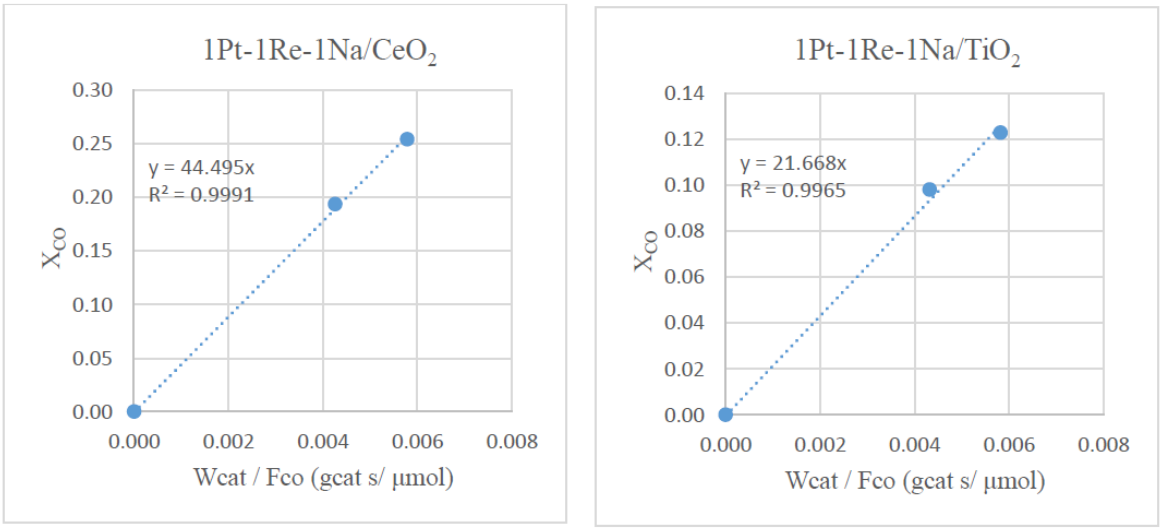

Figure A.15. A graph of CO conversion against residence time for Run #15 conducted at 350 ^{o}C over 1Pt-1Re-Na/CeO_2 (to the left) and 1Pt-1Re-1Na/TiO_2 (to the right)

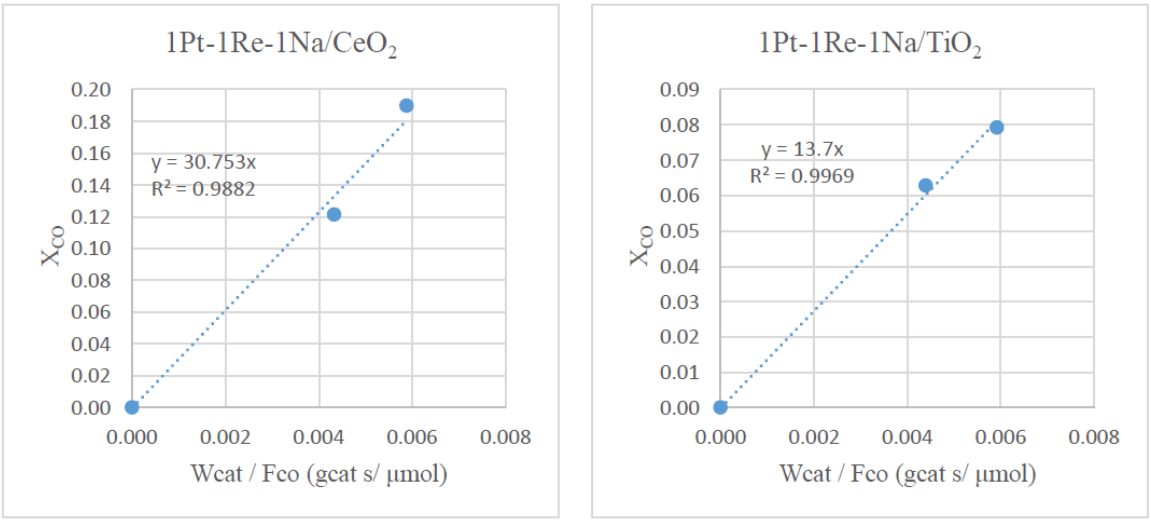

Figure A.16. A graph of CO conversion against residence time for Run #2 conducted at 325 ^{o}C over 1Pt-1Re-Na/CeO_2 (to the left) and 1Pt-1Re-1Na/TiO_2 (to the right)

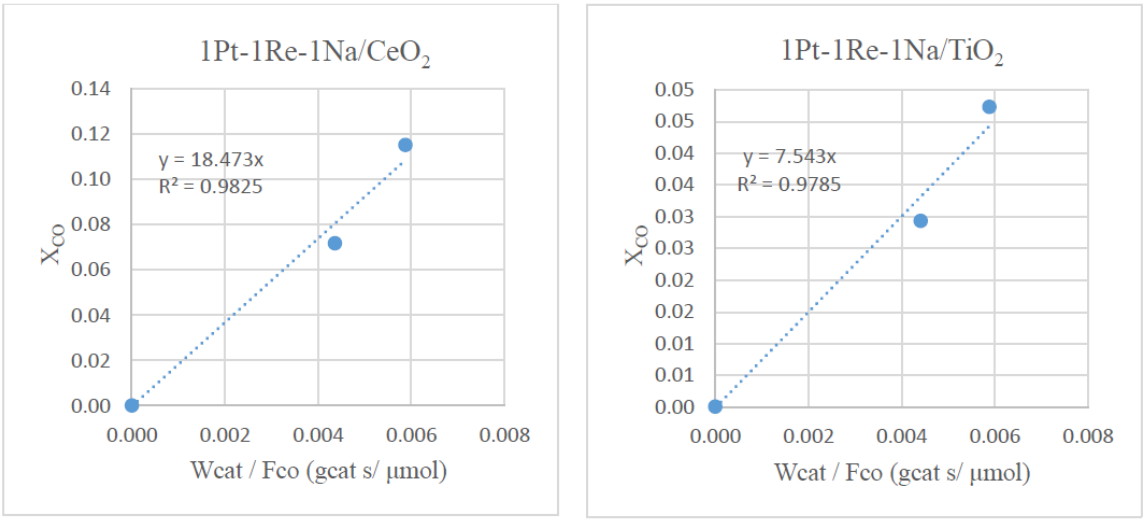

Figure A.17. A graph of CO conversion against residence time for Run #2 conducted at 300 ^{o}C over 1Pt-1Re-Na/CeO_2 (to the left) and 1Pt-1Re-1Na/TiO_2 (to the right)